An investigation into the performance of algorithms used to retrieve cloud parameters from LITE lidar data, and implications for their use with PICASSO-CENA lidar data.

Stuart A. Young

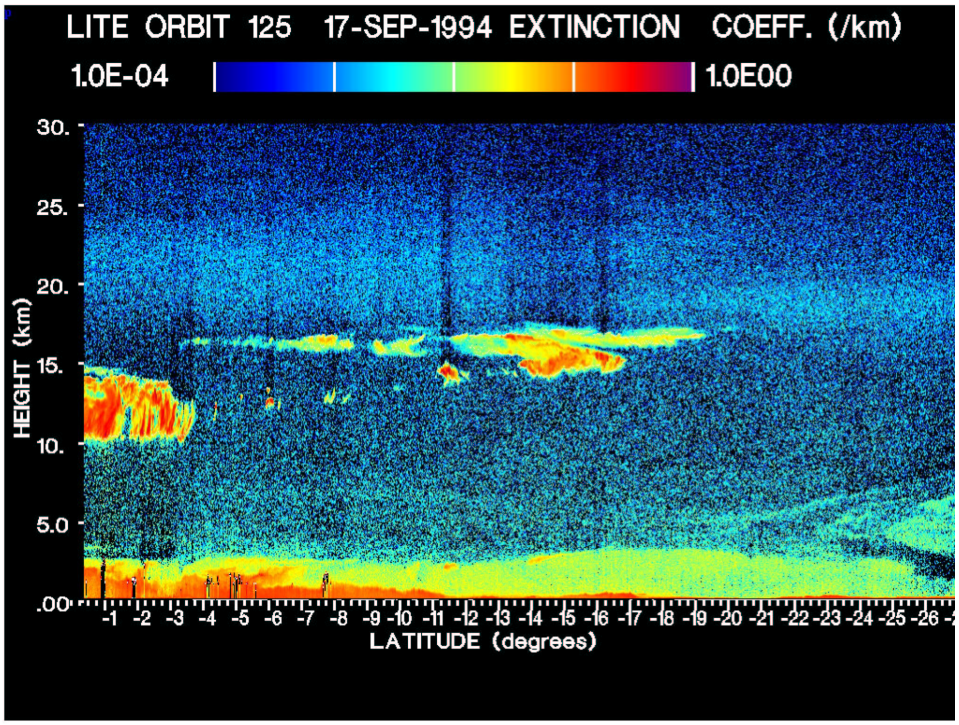

National Library of Australia Cataloguing–in-Publication Entry

Young, Stuart A.
An investigation into the performance of algorithms used to retrieve cloud parameters from LITE lidar data, and implications for their use with PICASSO-CENA lidar data.

ISBN 0 643 06647 0.

1. Remote sensing. 2. Clouds - Remote sensing.
3. Atmosphere - Remote sensing. 4. Algorithms.
I. CSIRO. Division of Atmospheric Research.
II. Title. (Series: CSIRO Atmospheric Research technical paper ; no. 53).

621.3678

CSIRO Atmospheric Research
PB 1, Aspendale, Victoria 3195, Australia
Ph: (+61 3) 9239 4400; Fax: (+61 3) 9239 4444
E-mail: chief@dar.csiro.au

CSIRO Atmospheric Research Technical Papers may be issued out of sequence. From July 2000, all new Technical Papers will appear on the Web site of CSIRO Atmospheric Research. Some Technical Papers will also appear in paper form.

A complete list of CSIRO Atmospheric Research Technical Papers can be found at
http://www.dar.csiro.au/info/TP.htm

Abstract

This document investigates the performance of various algorithms in the analysis of space-borne lidar data when used to retrieve profiles of extinction in clouds and aerosol layers. The retrieval of other parameters of interest, namely the effective optical thickness, lidar ratio (extinction-to-backscatter ratio) and the altitudes of the bases and tops of clouds is also studied. The algorithms were tested on simulated PICASSO-CENA lidar data under different vertical smoothing and horizontal averaging scenarios. The algorithms were then used to analyse selected LITE "scenes" to see how well they performed on real satellite lidar data. It was found that several enhancements the algorithms were required.

As it seems likely that a significant amount of averaging of consecutive lidar profiles will be required in order to improve the signal-to-noise ratio (SNR) sufficiently to permit the analysis of some features, the performance of two different averaging schemes was investigated using LITE data. These are the "average then retrieve" and the "retrieve then average" schemes. It was found that, provided the SNR was sufficiently high and the atmospheric feature did not change significantly over the averaging interval, good agreements were obtained between the methods. If significant changes in the atmospheric features occurred over the averaging interval, then inconsistencies were found in the results of the two methods. A method is proposed whereby changes in the atmospheric structure can be tested using a single parameter. Examples are given of the application of this method to LITE data.

During the development of the algorithms, a novel method was devised whereby scaled 1064-nm lidar data were used as surrogates for 532-nm data that had been saturated, or clipped, during the recording process. This method allows the complete 532-nm profile to be reconstructed and increases considerably the amount of high-gain, and otherwise high quality, LITE data that can be analysed.

1 Introduction

The LITE (Lidar In-space Technology Experiment) mission, flown on the Space Shuttle Discovery in September 1994, demonstrated the feasibility of flying a lidar in space for the study of clouds and aerosols. Building on the LITE experience, the launch of the PICASSO-CENA[1] (Pathfinder Instruments for Cloud and Aerosol Spaceborne Observations - Climatologie Etendu des Nuages et des Aerosols (an extended climatology of clouds and aerosols)) satellite, planned for 2003, will provide a wealth of information on the distribution and properties of clouds and aerosols over a wide area of the globe. Because the PICASSO-CENA instruments will orbit at an altitude of about 705 km, compared with the LITE altitude of about 250 km on the Shuttle, and because of other logistical constraints, the signal-to-noise ratio of the PICASSO-CENA data will generally be lower than that found in the LITE data. This has implications for the analysis of the new data set. In general, considerably more averaging, both within a given profile and of consecutive profiles, will be required to ensure useful results are required. The performance of various analysis algorithms under different smoothing and averaging scenarios is receiving considerable attention from a number of research groups in preparation for the development of the Algorithm Theoretical Basis Document (ATBD) for the PICASSO-CENA mission. Aspects of this work are the focus of the current paper.

[1] Note that, for legal reasons, the name "ESSP3" will replace "PICASSO" until a replacement is approved.

2 Methods

The methods most commonly used for the analysis of lidar data to retrieve profiles of extinction are the Klett (1981) and Fernald (1984) algorithms. Both methods assume a functional dependence on the two unknowns in the lidar equation, namely backscatter and extinction, and provide the solution to a differential equation of the Bernoulli type that is derived using the above assumption. The Fernald solution has a couple of advantages over the Klett solution. Although Klett (1985) did provide a method of considering two scattering components in the atmosphere, many researchers continue to use the single-component solution, even in circumstances where its use is inappropriate. The Fernald algorithm does consider both the molecular scattering component and the cloud or aerosol scattering component in a physically realistic way. It also expresses the solution in the form of a linear variable (the normalised, range-squared corrected received power) and this is more appropriate for use with low signal-to-noise ratio data where many data points have negative values. The Klett algorithm uses the logarithm of the same variable (but then expresses the solution in terms of an exponential function of this quantity), so encounters difficulties with noisy data containing negative data points.

However, as they stand, both algorithms are inappropriate for the analysis of lidar data measured from space. This results from the invalidity of the central assumption on which they are based, namely that the extinction coefficient can be expressed as some function of the backscatter coefficient. The problem is that, for lidar measurements at 532 nm, the main wavelength for both LITE and PICASSO-CENA, extinction arises not only from scattering but also from ozone absorption. Even during the moderate aerosol loading of 1994, just three years after the massive eruption of Mt Pinatubo, the ozone absorption was comparable with the aerosol scattering extinction throughout most of the stratosphere. (This is less of a problem at 355 nm, and insignificant at 1064 nm.) As it is likely that both LITE and PICASSO-CENA data will be calibrated in the “near field” of the lidar return, the region between the lidar and the first cloud or aerosol layer, ozone absorption needs to be considered. The above algorithms can only be used if the lidar signals are prescaled by the ozone absorption profile. In the investigations reported here, the Fernald algorithm included such prescaling. In addition to the modified Fernald algorithm, the present study considered a linear iterative scheme used for the analysis of ground-based lidar data by Gambling and Bartusek (1972a,b). This algorithm includes ozone absorption in the calculation of the attenuation profile. A forward, linear iterative algorithm is also being considered for the PICASSO-CENA ATBD by Vaughan et al. (2000).

Klett (1981) states that if an atmospheric feature has sufficient optical thickness, knowledge of the ratio of extinction to backscatter (the so-called lidar ratio) is unnecessary, and a solution initiated on the far side of the feature (a backward solution) will converge to the true profile of extinction. In many of the profiles measured by LITE, and those expected from PICASSO-CENA, this method is not suitable because of the often low signal-to-noise ratio (SNR) at those great ranges from the lidar, the complete attenuation of the lidar signal by some intervening cloud, or the fact that many clouds, like the thin cirrus so common in the tropics, have insufficient optical thickness to ensure adequate convergence. So a value of the lidar ratio must be found if extinction profiles are to be retrieved.

Values of the lidar ratio for a particular feature could be obtained from a data base that associates a particular cloud or aerosol type with a particular ratio. Atmospheric temperature, latitude, season, wavelength dependence, and depolarisation ratio are all possible candidates for categorising the range of appropriate lidar ratios. However, for optically-thin clouds, Young (1995) has proposed an analytical method whereby the effective optical thickness and

lidar ratio may be derived by measuring the reduction of the lidar signal on the far side of a cloud from the value in the absence of the cloud. The particular suitability of this method (hereafter referred to as the transmittance method) to thin cirrus has been reviewed by Nicolas et al. (1997). The performance of the method on data simulated for the (now cancelled) Japanese space lidar ELISE was reported by Liu et al. (2000). (Note that Sassen and Cho (1992) also derive a value of the lidar ratio by adjusting the ratio iteratively until the retrieved scattering ratio (the total backscatter derived by molecular backscatter) returns to unity in the 500 m above the cloud top.)

The work reported here investigated the performance of both the modified Fernald algorithm and the linear-iterative algorithm in obtaining profiles of extinction. The algorithms were used in conjunction with the method described by Young (1995) to obtain values of the lidar ratio when the data and targets were appropriate for this method. During the analysis of the LITE data, it was found that clouds were usually embedded in a background aerosol layer that extended from the surface through the stratosphere. The work of Young (1995) is further extended here to allow the retrieval of the effective cloud optical thickness and lidar ratio in these situations. Details of this method are presented in Appendix 1. In other cases, lidar ratios, typical of the target under study, were used in the retrievals instead. First of all the algorithms were tested on examples of simulated PICASSO-CENA lidar data (Powell, 2000). Various degrees of smoothing and averaging were used and the effects on the retrievals noted. Then attention was focused on actual lidar data measured during the LITE mission. Various types of scenes were studied, including both high- and low-gain nighttime data and daytime data, this sequence representing a general reduction in SNR.

During the study of the high-gain, nighttime data it was found that many profiles measured at 532 nm (and many also measured at 355 nm) were clipped during the digitisation process, and could not be analysed. This was unfortunate, as these data had by far the best SNR and, as the signal below the clouds could often be measured, were otherwise ideal for determining the effective optical thickness and lidar ratios directly from the data.

To see if these clipped data could be recovered and used, a separate study was made into the consistency of the relationship between the lidar signals at 532 nm and 1064 nm in regions where neither signal was clipped. Cirrus clouds proved to be the best targets for this exercise. Software was developed to plot, on height versus latitude axes, values of the corrected “colour ratios”, the ratio of the signal at 1064 nm to that at 532 nm, both suitably corrected for wavelength-dependent attenuation, to test the validity of the assumption that the cirrus particles are generally large enough so that scattering is independent of wavelength. This technique was applied to several LITE scenes containing a variety of clouds. Another investigation also considered the effect on this ratio of the attenuation by the cloud of the background molecular signal. The variation in the ratio over various LITE scenes was analysed. These methods are described in Appendix 2. As a result of these investigations, methods were incorporated into the analysis software to determine the calibration between the 532-nm and 1064-nm profiles using those unclipped 532-nm points and the corresponding 1064-nm points. The 1064-nm profile was then rescaled and the appropriate points substituted for the clipped 532-nm points in order to produce a complete 532-nm profile. The issue of the 1064-nm to 532-nm calibration is also receiving interest by other researchers for another reason. As the 1064-nm signal from air molecules is not measurable, data measured at this wavelength cannot be calibrated using the same techniques as used at 355 nm and 532 nm, by normalisation to the known molecular atmosphere above the stratosphere. Calibration of the 1064-nm signal by comparison with the 532-nm signal from cirrus clouds is being investigated as a possible solution and is showing some promise (J. Reagan, M. Osborn, private communication, 2000).

Software incorporating the methods and algorithms described above was written to allow their use with both LITE and PICASSO-CENA data. The various computer programs are described in Appendix 3.

3 Results

PICASSO-CENA

The analysis algorithms were tested on a variety of 532-nm PICASSO-CENA simulated data. The simulated data analysed included examples that presented a range of difficulty to the algorithms. Generally, the higher the optical thickness and the higher the extinction-to-backscatter or lidar ratio, the less accurate the retrievals. The main reason for this was that the greater the optical thickness of the cloud, the weaker and noisier the signals from below the cloud. This led to inaccurate estimations of the lidar ratio using the method described in Appendix 1, and the retrieved extinction profile was affected accordingly. In some cases the cloud was so optically thick there was no sub-cloud signal from the atmosphere. In these cases the lidar ratio could be estimated from the integrated attenuated backscatter as is commonly done, but the weak and noisy signal from the lower regions of the cloud led to uncertain estimations of optical thickness. In all cases, however, the uncertainties in the retrievals could be reduced by averaging more profiles before retrieving the desired parameters.

Examples of the analysis of three different cases are shown in Figures 1 to 3. These represent simulation cases 20, 21 and 27, with optical thicknesses of 0.5, 1.5 and 4.5 respectively. The respective lidar ratios were 44.3, 59.5 and 50.34 sr. The effects of averaging different numbers of profiles are shown in (a), (b) and (c). The single-profile data, shown in (a), are plotted using + symbols to indicate the noisiness in the raw signals. It can be seen in Figures 2 and 3 that very few photons are detected below the cloud and this causes large uncertainties in the fitting to the reference signal in this region. Note that in Figure 3 (a) and (b), the solution was terminated near cloud base either because there was either no signal to analyse or the estimated uncertainty in the retrieval has exceeded some specified limit. The results of these, and other analyses, are presented in Table 1 where the retrieved parameters are compared with the model values.

Note that, in order to increase the SNR of the data and to reduce the data volume, a significant amount of pre-processing will be done on the spacecraft before transmission to the Earth receiving station. This will include the pre-averaging of different numbers of profiles in different height regions. The composite signals from greater height regions will be the average of several profiles. The vertical resolution in these regions will also be reduced. For these reasons, in the PICASSO-CENA simulations, data are stored in “frames”. Each frame contains a different number of profiles for different height intervals in order to improve the SNR and to reduce the data volume. Typically there are 20 profiles for the lower altitude region, but only one profile, representing the average of 20 individual profiles, for the higher altitudes (above 19 km). In the analyses shown here, a “single-profile” represents the profile reconstructed from one profile of the lower region combined with the single profile for the upper region. As such, the resulting profile is only truly a single profile below about 19 km, but an average of 20 profiles above this height. This is obvious in the plots as a dramatic increase in noise below 19 km. The 20-profile data plotted in the panels labelled (b) are the average of all 20 of the lower altitude profiles combined with the single profile for the greater altitudes, so represent a true average of 20 profiles in both altitude regions. The increase in

SNR above 20 km in these plots results from the decreased height resolution and recorded bandwidth in this region. The 400-profile data are the averages of 20 major frames of data.

One obvious feature to note in all cases where 20 or fewer profiles are averaged is the non-Gaussian distribution of the signal where the count rate is low. This is particularly true below cloud base but also is noticeable in the near field of the signal at the maximum altitudes studied. This Poissonian distribution of the data affects the retrievals. This occurs because, in the method described in Appendix 1, the measured signal is fitted to the reference signal using linear regression, which assumes that data points are normally distributed about a mean value. This assumption of a symmetrical distribution of the data is obviously not valid in the regions of the signal where the count rate is low. A solution to this problem is to measure the signal baseline or offset independently, then use simple ratios instead of linear regression. This option was actually incorporated into the software used for the analysis of the LITE data described below, but was not used here so as to demonstrate the effect. (Note that the algorithms were originally developed for a lidar system limited by Gaussian-distributed thermal noise in the electronic amplifiers.)

LITE

After verifying the performance of the retrieval algorithms on the simulated PICASSO-CENA data, the performance was tested on a range of LITE data scenes. The scenes included examples of high-gain nighttime data, low-gain nighttime data and daytime data. These examples were taken from sections of LITE Orbits 125, 13 and 104 respectively. The LITE data differed considerably from the simulated data. Whereas the simulated data generally had isolated clouds or aerosol layers, each with constant values of extinction and lidar ratio, and at fixed altitudes, in the actual data all these parameters change. In addition, clouds were usually found embedded in a continuous aerosol layer.

Reference profiles

As explained in Appendix 1, reference cloud-free profiles were needed to allow the accurate determination of the cloud boundaries and to retrieve the desired cloud parameters. The calibration can also be achieved with considerably more accuracy than would be achieved if the measured signals had to be fitted to a purely molecular reference profile. This is because the reference profiles and the measured signals are similar, apart from the cloud layers in the latter. This allows the fitting to take place over a much larger altitude range (typically from 40 km down to the top of the first cloud layer) than if calibration were limited to the 30 to 40 km altitude region where fitting to a molecular reference is valid. The signal in the higher region is much lower and the resulting fitting coefficients far less precise. Reference profiles were produced by averaging lidar signals in several latitude regions in Orbit 125. These reference profiles are plotted in Figure 4 (a) normalised between about 30 to 40 km altitude, to the signal expected from a purely molecular atmosphere. The molecular profile was calculated from the meteorological data stored in the LITE data record, and from a latitude-dependent, reference ozone file obtained from the NASA PICASSO-CENA simulation team. Figure 4(b) shows these profiles as ratios of the reference signal to the molecular signal that are, effectively, attenuated scattering ratios. The reference profiles were solved for profiles of aerosol backscatter and transmittance, and these were used during the analysis of the scenes. Aerosol extinction to backscatter ratios (lidar ratios S_A) of 40 sr were assumed. As the aerosol optical thickness is low, this value could be varied over a considerable range without changing the retrieved backscatter profile significantly. The profiles in Figure 4 have been subjected to vertical smoothing with a Gaussian function having a width (plus and minus one standard deviation) equal to 33 data points (495 m).

To show how well the individual profiles can be fitted to the reference profile, the fitted signals, rescaled and plotted on height versus latitude axes, are plotted in Figure 5. The plotted variable is the ratio of the measured signal to the reference signal. Data are for latitudes from the equator to about 7^o S during Orbit 125. No horizontal or vertical smoothing has been used. This format allows one to read directly the transmittance (squared) of the thicker clouds by studying the colour scale in the regions below the clouds. The pale green colour represents a ratio of unity, and it can be seen that the maximum scattering ratios are in the range 30 to 100, and the minimum of the square of the cloud transmittance, about 0.1, equivalent to an optical thickness of about 0.6). The dark band at an altitude of about 2 km is an artefact resulting from the inclusion of a low cloud in the reference profile shown in Figure 4. Note that this reference profile is not used to detect clouds below a lower limit set here at 3.5 km.

Analysis of LITE scenes

The first step in the analysis of the signals is the detection of the cloud boundaries. The ratio method described in Young (1995) was used for this purpose initially. However, it was found that this method required frequent tuning, or selection of different threshold ratios, for the reliable detection of clouds where the SNR changed from scene to scene or where a different amount of averaging was used. Another method was tested with some success. In this alternative method the signal was fitted to the reference signal in the clear region using linear regression as before. In the test region, the cloud boundary was defined as the first of n consecutive points where the difference in the signal and the linear extrapolation of the fit exceeded the uncertainty in the extrapolation of the fit by a selectable factor of m. The uncertainty in the extrapolation was calculated from the uncertainties in the coefficients of the fit. These uncertainties were related to the SNR in the data and varied with the averaging scheme used. As the SNR and the averaging scheme (vertical and horizontal) varied considerably in the analysis of the LITE data, the reduction in the required adjustment of the detection parameters was a considerable benefit.

The analysis then proceeded as described in Appendix 1. The fitting coefficients above and below the cloud, as measured in the cloud detection algorithm, were used to determine the calibration factor, the effective optical thickness and effective lidar ratio, ηS_C, and the uncertainties in these quantities. If the value of ηS_C derived in this process fell outside acceptable limits it was set at either the minimum or maximum value of the limit range, depending on the value of ηS_C .

A forward analysis algorithm, either a linear iterative algorithm or a modified, two-component, Fernald extinction algorithm, was then used with these quantities to retrieve a profile of extinction. Points in the retrieved profile with backscatter five times the molecular value were assumed to be cloud signals and were assigned a lidar ratio of ηS_C, otherwise the lidar ratio was set at that of the background aerosol, S_A. The value used for S_A was 40 sr in the stratosphere (Young and Osborn, 1998), with the same value used in the free troposphere. A value of 20 sr was used for regions below some minimum altitude, where the signal exceeded some critical value. Such points were assumed to be boundary-layer aerosols and clouds.

The solution was checked at each point in the profile being analysed to ensure that it was not diverging. This is done most easily in the Fernald algorithm by testing the sign of the denominator. An additional test in either algorithm was to see if the retrieved extinction exceeded some limit (e.g. 30 km^{-1}). If the solution was diverging, then the value of ηS_C was reduced until it reached the lower limit of the acceptable range, after which the calibration factor was adjusted instead. (This approach was adopted in an attempt to correct for possible

errors in the calibration factor. Divergence of the solution not only results from an incorrect value of ηS_C. It can also result from an incorrect calibration factor or signal baseline (offset) removal.) Note that, because the current cloud detection algorithm only detects one cloud layer, a broad window was set to include only the clouds of interest. Lower clouds, particularly those in the boundary layer, were excluded from this divergence checking process. A quite different value of ηS_C would be expected for these clouds, and most of the signals were saturated in the scenes studied, so any adjustment would have been of little validity.

Because of the uncertainties in the evaluation of ηS_C, the extinction solutions varied considerably from profile to profile. Two solutions to this problem were implemented. In cases where the optical thickness was very low and the uncertainty in ηS_C high, a default value of ηS_C was used. Even in cases of higher optical thickness, small errors in ηS_C often caused considerable variation in the retrieved aerosol backscatter in the sub-cloud layer. A dramatic improvement was achieved by using a second iteration loop. This measured the average value of the retrieved aerosol backscatter in the sub-cloud layer (that between cloud base and the lower boundary of the window described above) and compared this value with the average of the aerosol backscatter in the same region of the reference profile. The calibration factor and the lidar ratio for the cloud layer were adjusted within their limits until a match was found within the uncertainties of the averages. At present the method for making this adjustment is not very refined and could well do with further development. (See recommendations below.)

The result of the analysis for the same region of Orbit 125 as shown in Figure 5 is presented in Figure 6. Note that most of the 532-nm signals in the cloud regions were clipped in the original data, but the data points have been replaced with suitably-scaled 1064-nm data points using the novel approach described in Appendix 2. The data are unsmoothed in height and are single-profile retrievals. No running mean of consecutive profiles has been used in this plot. The value of ηS_C was retrieved as described above. Note the excellent, profile-to-profile consistency in the retrieval of the extinction in both the cloud layers and the aerosol layers. Figures 7, 8 and 9 show similar plots for the next three latitude intervals in the LITE 125 Orbit. As the clouds in these regions had low optical thicknesses, and the retrieved value of ηS_C had large uncertainties, a default value of 30 sr was used in retrieving the cloud extinction profiles.

The retrieved calibration factor, effective optical thickness and lidar ratio for each of the 4800 lidar profiles contained in the Orbit 125 data presented in Figures 6 to 9 are shown in Figure 10. For the latitude region up to about 7 degrees, the value of ηS_C was determined by the methods described above. For subsequent latitudes, it was set at a default value of 30 sr, but was allowed to vary along with the calibration factor, in order to match the aerosol backscatter in the sub-cloud layer as described above. Values of ηS_C of 40 sr correspond to regions where no cloud was detected. It can be seen that most variation in ηS_C and the calibration factor occurs where thicker cloud was detected. A few spuriously high values of the calibration factor can be seen. These occurrences are unexplained at this stage but it is thought that they may result from incorrect values of the baseline value causing the calibration factor and lidar ratio to be adjusted inappropriately. This is discussed later. The plot of effective optical thickness indicates that the method works well at these SNRs for optical thicknesses in the approximate range 0.01 to at least 0.8.

Figure 11 compares the integrated attenuated cloud backscatter, $\gamma'_C(\pi)$, and effective cloud optical thickness. When Equation 10 in Appendix 1 is fitted to the data, a value of 18.56 ± 0.14 sr is found for the effective lidar ratio.

The data studied so far have been nighttime data. Next we consider the performance of the algorithms on daytime data where the SNR is much lower. It was found that it was not possible, in general, to retrieve cloud optical parameters from single-profile daytime data. Success was only achieved by using a combination of vertical smoothing and running means of consecutive profiles. Examples of such analyses are presented in Figures 12 and 13 where a section of LITE Orbit 104 is shown. Because of the low SNR in the data and the lack of sufficient cloud-free profiles to produce reference profile of good quality, the reference profile calculated from similar latitudes in Orbit 125 was used. In Figure 12, individual profiles have been smoothed with a window of seven points (105 m) and running means have been constructed from 50 consecutive profiles before the analysis algorithms were initiated. The SNR was improved sufficiently to allow the determination of the calibration factor, effective lidar ratio and optical thickness. Saturation has occurred in some patches of low cloud and the solution below these regions is blacked out. Figure 13 shows the analysis of the same region of Orbit 104, but here only 10 consecutive profiles are used in the running mean. The SNR is too low to permit the determination of the cloud parameters as before. It is so low, in fact, that a reliable calibration could not be achieved by fitting to a reference profile, although cloud boundaries were found accurately. Analysis was performed using a fixed value of the lidar calibration factor and a default value of lidar ratio of 30 sr in the clouds. Figure 14 shows the variations in the retrieved quantities when using the 50-profile running means as in Figure 12. Figure 15 is a scatter plot of the integrated attenuated cloud backscatter against the effective cloud optical thickness for the same analysis. An effective cloud lidar ratio of 16.0 ± 0.2 sr is determined by fitting Equation 10 in Appendix 1 to the data.

Averaging schemes

It is apparent that a degree of averaging is needed before analysis of all but the highest quality data can proceed. However, averaging of consecutive profiles is only valid if the atmospheric structure does not change significantly from profile to profile. Because the lidar equation depends on both a backscatter factor and an attenuation factor that is an exponential function of the integral of the extinction (the backscatter scaled by the lidar ratio), a simple arithmetic average of consecutive lidar profiles will not, in general, preserve the relationship between the backscatter and the extinction. A comparison was made, therefore, of the results of averaging consecutive profiles and then retrieving a profile of extinction, with the results of retrieving extinction profiles from individual profiles first then averaging the solution profiles. These schemes are referred to, respectively, as the “average then retrieve” and the “retrieve then average” schemes. It should be noted also that, even if the atmosphere were to remain constant, the performance of the cloud detection, calibration and cloud parameter estimation algorithms is affected by the SNR of the data, and a variation in the results of the schemes would be expected.

Comparisons between the “average then retrieve” and the “retrieve then average” schemes are presented in Figures 16 to 22 where various sections of the LITE Orbit 125 data are analysed. The structure of the clouds in latitude regions in the figures can be inspected in Figures 6 to 9. Figures 16 and 17 show a similar region of thick cirrus; the former is an average of 100 profiles while the latter is an average of 25 profiles. The agreement of the extinction profiles in the region of the cloud is excellent in both cases, as is the agreement of the derived parameters (lidar system (or calibration) constant, effective optical thickness and lidar ratio). It is interesting to note that a greater discrepancy occurs between the retrieved aerosol extinction profiles in the boundary layer. This is explained by the presence of a thin cloud signal on a small number of profiles. When subjected to a running mean, the effects of this cloud are smeared across several profiles, while a few individual retrievals will be affected.

Figure 18 also shows good agreement between the two schemes using averages of 25 profiles. Generally good agreement is achieved both in the cloud layer and in the stratospheric and tropospheric aerosol layers.

An example of the analysis of in a region where the cloud vertical structure is varying is shown in Figure 19. Significant differences are seen in the retrieved extinction profile and in the retrieved parameters. The lidar ratios retrieved by the schemes are quite different and lead to different extinction profiles.

An example of a case where the cloud structure is relatively constant but the SNR is low is shown in Figure 20 where the cloud signal is considerably weaker than in the previous examples. Although the calibration was achieved more precisely with the "average then retrieve" scheme, the other parameters could not be obtained with any precision. Because the optical thickness of the clouds was so low, the resulting, small decrease in the signal below the cloud was too low to be measured above the noise using the transmittance method, even in the averaged profile, and a value of zero is shown for this parameter in Figure 20. Statistical fluctuations in the single profiles analysed in the "retrieve then average" scheme allowed the cloud optical thickness to be determined occasionally, but the uncertainty is very high. In both analysis schemes, if the optical thickness cannot be determined using the transmittance method, or falls outside the acceptable range, it is assigned a default value, here 30 sr. This value may be further adjusted to ensure that the solution does not diverge, or to match the measured and calculated optical thicknesses (Young, 1995). It can be seen that the close agreement shown here between the lidar ratios determined with both schemes arises merely because the same default value was used. The difference in the calculated optical thicknesses arises mainly from the fact that the cloud detection algorithm, when processing the low-SNR single profiles in the "retrieve then average" scheme, could not detect reliably the cloud base at 15.5 km, and found an average value of 16 km instead. Differences exist in the retrieved extinction profiles, and they increase with penetration through the cloud. These differences are shown on an expanded scale in Figure 21.

Note that discrepancies between the averaging schemes are expected to occur mainly in the retrieval of cloud profiles. An example of the comparison of the averaging schemes when applied to aerosol data is shown in Figure 22. As aerosol layers tend to vary more slowly, discrepancies are likely to be less pronounced. In addition, because of their low optical thicknesses, it is not possible to derive accurate values of the lidar ratios of aerosol layers directly from the data using the methods of Appendix 1 or other methods. Therefore, default values of the lidar ratio would normally be used, thus removing one source of possible discrepancy. The low optical thickness of aerosol layers means that the solution is driven mainly by the backscatter coefficient and is only weakly dependent on the lidar ratio anyway. (These statements would obviously need to be modified if a major volcanic eruption were to inject a strong aerosol layer into the upper atmosphere.)

An indicator of cloud profile variability

From the above examples it is obvious that a simple indicator is required for determining when changes in the cloud structure are significant enough to affect the average of consecutive profiles. The method needs to be fairly simple so as not to impose too heavy a load on the real-time processing of PICASSO-CENA data. A possible option is to calculate the correlation coefficient between consecutive profiles, or between the running mean and the next profile to be measured. The calculation could cover the whole profile or could be subdivided into height zones of interest or zones where change is most likely to occur. This method was explored only briefly, but the results presented in Figure 23 for Orbit 125 and Figure 24 for Orbit 104 show considerable promise. As can be seen by comparing these

figures with the retrieved extinction plotted in Figures 6 and 12, the correlation coefficients show very large changes when the structure of the cloud changes. The correlation coefficients are low in the clear regions because the SNR in these regions is lower than in the cloudy regions. The signal (and SNR) in the clear regions in the nighttime data (Figure 23) is high enough that the correlation between successive profiles does not drop to zero. In the daytime, low-gain data (Figure 24) there is little detectable signal and the noise in successive profiles is uncorrelated in these regions, so the correlation drops to zero for the cloud-free profiles.

4 Conclusions

The work reported here allows the following conclusions to be reached:

1. Algorithms have been developed that successfully retrieve profiles of extinction in both simulated PICASSO-CENA and actual LITE data sets.
2. For the LITE data, a cloud-free reference profile was needed to permit the accurate retrieval of the cloud parameters.
3. In cases of high to moderate SNR, the additional quantities of the calibration factor, effective optical thickness and effective lidar ratio for the cloud layer can be determined.
4. In cases of low SNR, profiles and parameters can be retrieved successfully if the SNR is improved by averaging several consecutive profiles.
5. Comparisons of the "retrieve then average" scheme with the "average then retrieve" scheme show

- good agreement between the schemes when the SNR is high and consecutive profiles are consistent and poorer agreement if either of these conditions is not met,
- generally good agreement between aerosol profiles retrieved with both schemes.

6. Dramatically improved consistency is achieved between consecutive retrieved profiles by using a double iteration, involving the cloud retrieval and the sub-cloud aerosol layer.
7. Iteration schemes should include the lidar ratio, calibration constant and signal baseline or offset.
8. For the LITE cases studied, the ratio of the 1064-nm to 532-nm signals was consistent enough to permit the replacement of saturated 532-nm data and the reconstruction of complete 532-nm profiles that could be analysed to give credible results.

5 Remaining issues and recommendations for further development

During the development and testing of the algorithms and the analysis of the LITE data, it became apparent that further developments were needed over what had been satisfactory for the analysis of the PICASSO-CENA simulation data. Some were incorporated as described above, but others required more time than was available for implementation. The issues are very relevant to the analysis of the PICASSO-CENA data, and will need to be considered in the ATBD. Some of these points are described below.

1. An algorithm needs to be developed to optimise the automatic selection of the lidar ratio and the calibration constant in those cases where the solution is diverging in either the positive or negative directions. In the present software, these variables are only weakly linked. The lidar ratio is iterated by the main SOLVE subroutine in order to match the calculated optical thickness with the measured value. It is also reduced by the extinction algorithm subroutine if the solution is diverging in the cloud. The calibration constant is also adjusted by the same subroutine. At present there are two such subroutines, FERNALD and LINITER, and these are called by SOLVE. These subroutines adjust the calibration constant in those cases where it is desired to force the retrieved, sub-cloud, aerosol extinction to match the average value in the same region of the reference profile. At present it is possible, under some circumstances, for the values of both the lidar ratio

and the calibration constant to be adjusted outside acceptable limits, and physically unrealistic results ensue. For real-time PICASSO-CENA data, it is possible that a third variable, the signal offset or baseline value, may also need adjustment. A parameter search routine needs to be developed to arrive at the optimum values of each of the three parameters. As each parameter has an expected probability distribution, the search path should be directed by the combined probabilities of the variables. The combination of parameters selected should be the one that produces the desired result and has the highest combined probability. Note that the baseline value is usually determined in regions where the signal is small. As these regions have low photon count rates, the probability distribution of the values is distinctly Poissonian and not Gaussian. The degree to which the assumption of a Gaussian distribution leads to the estimation of an incorrect baseline value needs investigation.

2. At present, the cloud detection algorithm is only set up to detect an isolated cloud layer in a broad altitude window. The solution algorithms assign the same lidar ratio to all points in the region between the detected cloud boundaries. If there are more clouds in the detection window, it is sometimes inappropriate to assign the same lidar ratio to all the cloud layers. A more sophisticated cloud detection algorithm and lidar ratio assignment algorithm needs to be incorporated into the existing software. (Note that the feature-finding algorithms being considered for PICASSO-CENA are more sophisticated than the one used here, but will still need to consider the situation described.)

3. One of the conclusions of this work is that a significant amount of averaging of consecutive profiles is needed in order to retrieve useful results. However, averaging over dissimilar profiles can lead to physically meaningless outputs. The averaging algorithm needs to be able to detect when there has been a significant change in the profiles, and to adjust the averaging windows accordingly. One method may be to calculate the correlation coefficient for different height regions of consecutive profiles. A significant drop in the correlation would indicate that the profiles have changed. Examples of how this might work are illustrated in Figures 23 and 24, which show the variation in the linear correlation coefficient between consecutive profiles. The changes in correlation in these figures can be clearly related to the changes in cloud structure seen in Figures 6 and 12.

4. At the time of writing LITE data, converted to PICASSO-CENA format and resolution, were not available for analysis, although they are expected to be available soon. In order to make direct comparisons with LITE retrievals at full and reduced resolution and SNR, the existing software needs extensions to accept the new data format for the simulation data, then the data need to be analysed.

6 Acknowledgments

The author gratefully acknowledges financial support for this work from the Department of Atmospheric Sciences, Colorado State University (Prof. Graeme Stephens) and Martin Platt, through contract number P.O. # 304253.

The computer software developed by the author makes extensive use of menu and other data input features contained in libraries written by Denis O'Brien (CSIRO Atmospheric Research). The rapid, on-screen inspection of data during various stages of processing is made possible by in-program plotting libraries, also provided freely by Denis O'Brien.

The author thanks Kathy Powell (NASA LaRC) for advice on details of her simulations of PICASSO-CENA data.

Mary Osborn and Mark Vaughan (both of NASA LaRC) explained the intricacies of various aspects of the calibration of the LITE data.

Mark Vaughan and Dave Winker (also NASA LaRC) have provided a stimulating interaction and discussions on various aspects of this work.

The LITE data used in this document were obtained from the NASA Langley Research Center Atmospheric Sciences Data Center.

7 References

Fernald, F. G. (1984). Analysis of atmospheric lidar observations: some comments. *Appl. Opt.,* **23**(5), 652-653.

Gambling, D. and K. Bartusek (1972a). Lidar observations of tropospheric aerosols. *Atmos. Environ.,* **6**(3) 181-190.

Gambling, D. and K. Bartusek (1972b). Discussions: Lidar observations of tropospheric aerosols. *Atmos. Environ.,* **6**(11) 869-870.

Klett, J. D. (1981). Stable analytical inversion for processing lidar returns. *Appl. Opt.,* **20**(2) 211-220.

Klett, J. D. (1985). Lidar inversion with variable backscatter / extinction ratios. *Appl. Opt.,* **24**(11) 1638-1645.

Nicolas, F., L. R. Bissonnette and P. H. Flamant (1997). Lidar effective multiple-scattering coefficients in cirrus clouds. *Appl. Opt.,* **36**(15) 3458-3467.

Platt, C. M. R. (1979). Remote sensing of high clouds Part I: Calculation of visible and infrared optical properties from lidar and infrared radiometer measurements, *J. Appl. Meteor.*, **18**(9) 1130-1143.

Powell, K. (2000). PICASSO-CENA data simulation website.
http://www-lite.larc.nasa.gov/pc_sims/l_select_simulations.html.
Reading software package available at
http://www-lite.larc.nasa.gov/pc_sims/idl_prog.html.

Sassen, K. and B. S. Cho (1992). Subvisual-thin cirrus dataset for satellite verification and climatological research. *J. Appl. Meteor.*, **31**(11) 1275-1285.

Vaughan M., (and other members of the PICASSO-CENA Lidar Scientists Working group (2000). Lidar Level II Algorithm Theoretical Basis Document. Ver00. 2000.17.31. (Available from M. Vaughan, NASA Langley Research Center.)

Young, S. A. (1995). Analysis of lidar signals from optically-thin clouds, *Appl. Opt.,* **34**(30) 7019-7031.

Young, S. A. and M. T. Osborn (1998). Comparisons of LITE observations with ground-based lidar and SAGE II profiles over SE Australia, In: Singh, U. N., Ismail, S., and Schwemmer, G. K. editors, *Nineteenth International Laser Radar Conference. Abstracts of papers; 1998, Annapolis, MD.* Hampton, Va., NASA, 1998, (NASA conference publication-1998-207671/PT2). pp 963-966.

Zhaoyan Liu, P. Voelger and N. Sugimoto (2000). Simulations of the observation of cirrus and aerosols with the Experimantal Lidar In Space Equipment system. *Appl. Opt.,* **39**(18) 3120-3137.

Appendix 1: Retrieval of cloud effective optical thickness and lidar ratio for clouds embedded in an aerosol layer

The method presented here is an extension of the work of Young (1995) who considered isolated clouds either in a clear atmosphere or above or below aerosol layers. Here it is assumed that the aerosol background extends from the surface through the stratosphere. This method is appropriate for space-borne lidars that experience a lower dynamic range than ground-based lidars, and also to other lidars with the capability of making high-sensitivity measurements throughout the atmosphere. In essence, the method relies on the production of a reference profile that represents the signal that would be measured from the atmosphere if no clouds were present, and the comparison (or fitting) of the measured signal with the reference signal on both sides of a cloud layer. The comparison on the near side corrects for any variations in the lidar calibration factor and the ratio of the fits obtained on the far and near sides of the cloud give the square of the effective cloud transmittance detected by the lidar. The steps in the method are described below.

1. A signal representing the lidar return from a purely molecular atmosphere is synthesised using molecular density and ozone data:

$$M(r) = \beta_M(r) T_M^2(0,r) T_{O3}^2(0,r) / r^2, \quad (1)$$

where β is the backscatter coefficient and T is the transmittance. The subscripts M and $O3$ refer to molecules and ozone respectively.

2. The reference profile is obtained, either from lidar measurements in cloud-free regions. (Alternatively, a model or other (e.g. SAGEII) aerosol profile data could be used to create a suitable profile.) This profile includes contributions from both molecular and aerosol scattering:

$$A(r) = C(\beta_M(r) + \beta_A(r)) T_M^2(0,r) T_{O3}^2(0,r) T_A^2(0,r) / r^2 + B + N_r(r), \quad (2)$$

where C is a system constant, B is a signal offset or baseline value, $N_r(r)$ is the statistical noise in the signal and background at range r, and the subscript A refers to aerosol.

3. The reference profile is calibrated by fitting over some altitude range where there is negligible aerosol scattering, to the molecular profile in 1. This can be done by simply finding the mean value of the ratio of the points of $A(r)$ to the corresponding points in $M(r)$ if the baseline term is known and removed. Alternatively, a linear regression of the corresponding point pairs gives values of the system constant, the baseline value and the uncertainties in both. These uncertainties, which mainly arise from $N_r(r)$, can be used later in estimating the uncertainties in the retrieved parameters. The result of this step is a calibrated reference profile:

$$R(r) = (A(r) - B) / C. \quad (3)$$

4. The reference profile is solved for profiles of the aerosol backscatter coefficient, $\beta_A(r)$, and transmittance $T^2_A(0,r)$ using model values of the lidar ratio for aerosols, S_A. These profiles are needed later.

5. Now, in the analysis of each lidar signal profile, an edge detection algorithm finds the ranges of the cloud top and base, r_t and r_b. The measured signal is then calibrated by

fitting to the reference profile using all the data points in the range interval between the lidar and the top of the cloud, being sure not to include any cloud points. It is in this step that the considerable advantages of using a reference profile are apparent. In Figure A1-1, the signal profile is fitted to the reference profile over the whole altitude range from 15 to 40 km. In addition to the cancellation of the broad aerosol feature at 22 km, the calibration is significantly more accurate than if it had been limited to the aerosol-free region above about 30 km. The contribution of the noise to the uncertainties in the calibration is reduced by fitting over a larger range of altitudes and, importantly, the signal near 15 km is one to two orders of magnitude greater than that above 30 km. Both factors contribute to a better calibration. This gives the calibration factor $CT^2(0,r_t)$ and the baseline value *B*. Here the transmittance factor includes the molecular, ozone and aerosol transmittance factors. By repeating the calibration in a cloud-free region below cloud base, and finding the ratio of the two calibration factors, we obtain a value of the cloud transmittance, $T_C^2(r_t, rb)$. The measured signal is

$$P(r) = C(\beta_M(r) + \beta_A(r) + \beta_C(r))T_M^2(0,r)T_{O3}^2(0,r)T_A^2(0,r)T_C^2(0,r)/r^2 + B + N_S(r), \quad (4)$$

where $P(r)$ is the measured signal power and $N_S(r)$ the noise at range *r*, and the subscript *C* refers to cloud. On fitting to the reference profile, $R(r)$, over the range *0* to r_t, removing the offset and calibrating we have

$$(P(r)r^2 - B)/CT^2(0,r_t) = (\beta_M(r) + \beta_A(r) + \beta_C(r))T_M^2(r_t,r)T_{O3}^2(r_t,r)T_A^2(r_t,r)T_C^2(r_t,r). \quad (5)$$

Dividing by the known transmittance factors, $T_M^2(r_t, r)$, $T_A^2(r_t, r)$ and, $T_{O3}^2(r_t, r)$, gives

$$\beta_T(r)T_T^2(r_t,r)/[T_M^2(r_t,r)T_{O3}^2(r_t,r)T_A^2(r_t,r)] = (\beta_M(r) + \beta_A(r))T_C^2(r_t,r) + \beta_C(r)T_C^2(r_t,r). \quad (6)$$

Here the subscript *T* implies "total", that is molecular, aerosol and ozone. But we know the transmittance through the whole depth of the cloud, $T_C^2(r_t, rb)$, from step 5, and can express this transmittance as a function of the mean extinction coefficient over the cloud depth.

$$T_C^2(r_t,r_b) = \exp\{-2\int_{r_t}^{r_b}\sigma_C(r)dr\} = \exp\{-2\sigma_C(r_b - r_t)\}. \quad (7)$$

Note the distinction between the mean value, σ_C, and the profile value $\sigma_C(r)$.

6. Now we make the following approximation to enable us to calculate the transmittance as a function of range at each point in the cloud:

$$T_C^2(r_t, r) = \exp\{-2\sigma_C(r - r_t)\}. \quad (8)$$

By substituting (8) into (6) and rearranging we have

$$\beta_C(r)T_C^2(r_t,r) = \beta_T(r)T_T^2(r_t,r)/[T_M^2(r_t,r)T_{O3}^2(r_t,r)T_A^2(r_t,r)] - (\beta_M(r) + \beta_A(r))\exp\{-2\sigma_C(r - r_t)\} \quad (9)$$

and, on integrating this function, the attenuated cloud backscatter, through the depth of the cloud, we define the integrated attenuated cloud backscatter:

$$\gamma_C'(\pi) = \int_{r_t}^{r_b}\beta_C(r)T_C^2(r_t,r)dr = \frac{1}{2\eta S_C}\left[1 - T_C^2(r_t,r_b)\right]. \quad (10)$$

The effective lidar ratio for the cloud, ηS_c, (Young, 1995) where η is a factor that approximates the effects of multiple scattering in the cloud as described by Platt (1979), is obtained by reorganising (10):

$$\eta S_C = \frac{1}{2\gamma_C'(\pi)}\left[1 - T_C^2(r_t, r_b)\right]. \tag{11}$$

Appendix 2: Use of 1064-nm LITE data to replace saturated 532-data. Calibration of 1064-nm data by comparison with the 532-nm signals from cirrus clouds.

During the recording of signals from many of the thicker clouds at high gain, the signal exceeded the input voltage range of the digitiser, and the data are saturated or "clipped". Unfortunately, it is just these data that offer the best opportunity of retrieving optical thickness and lidar ratio information, as the signal below the clouds is usually measurable and the clouds have sufficient optical thickness to allow a retrieval with low uncertainties. As the saturation only occurred on the 532-nm and 355-nm channels, with the weaker 1064-nm signal remaining unsaturated, some tests were devised to see if the 1064 nm signal could be used as a substitute for the saturated data. First, a simple method was devised, based on two assumptions:

1. The particles in the clouds under consideration (mainly cirrus) are large enough that backscatter and extinction and, as a consequence, transmission losses due to cloud extinction at both wavelengths do not differ significantly.
2. The cloud backscatter signal is very much greater than the combined molecular and aerosol signals.

The method can be summarised as follows (with symbols as defined in Appendix 1):

1. Define a height window where the clouds are likely to be located (5 km to 20 km)
2. Determine the saturation level for signals at each wavelength. (Because of ripple effects and baseline removal, this is not necessarily constant.)
3. Select pairs of points from each of the 532-nm and 1064-nm channels that are inside the height window, and are not saturated.
4. Scale the signal at each point by the molecular (including ozone) transmission losses between the satellite and the altitude of that range *r* and the calibration factor at that wavelength:

   $S_\lambda(r) = P_\lambda(r)/[C_\lambda T^2_{M,O3,\lambda}(0,r)]$,

   where *P(r)* is the data array *profile* and *C* is the calibration factor in the LITE data sets and $T^2_{M,O3,\lambda}(0,r)$ is the molecular and ozone transmittance from the lidar to range *r*.
5. Perform a linear regression of the 1064-nm points to the 532-nm points of the form $S_{1064}(r) = A + B.S_{532}(r)$.
6. In the 532-nm profile, substitute the saturated points with values estimated from the scaled 1064-nm data,

   $S^*_{532}(r) = (S_{1064}(r) - A)/B$.

The obvious limitation with the method is the validity of the second assumption above. While the aerosol and molecular scattering at 1064 nm in the 5-km to 20-km region is very much less than the cloud scattering, this is not always true at 532 nm. (The problem at 355 nm is even more acute.) The result is that the 532-nm signals in steps 4 and 5 above contain aerosol and molecular scattering, variously attenuated by the cloud extinction depending on the altitude of the point. So points near the top of the cloud have a larger molecular and aerosol offset than those points near the bottom of the cloud, and this causes an additional spread in the data points, over that resulting from signal noise. Nevertheless, it is informative to look at the results of this simple analysis. Figure A2-1 shows the variation in the fitting coefficient *B* obtained using the 1064-nm and 532-nm data for LITE Orbit 125 between latitude –0.46 and latitude –20.57.

It can be seen that the ratio (more correctly the B slope coefficient described above) is about 50 in regions where the cloud is thick. The cloud in the region between 0 and about -3.5 degrees latitude is thick cirrus between 10 km and 15 km. The cirrus between about -13 and -17 degrees latitude is thinner (possibly less strongly scattering) and lies in the height region between 14 and 17.5 km. There is some indication that the mean value of the fit is slightly higher for the higher cloud layer, although this is difficult to assess given the contamination of the cloud signals with molecular and aerosol scattering.

In an attempt to overcome the limitations of the simple approach, namely that the signals include significant amounts of molecular or aerosol backscatter, use was made of a reference profile produced as described in Appendix 1. This reference profile was used in two main ways. Firstly, it was used in determining cloud and non-cloud regions on any individual profile. Second it was used to subtract the aerosol and molecular contributions from data to be used in determining the scaling of the 532-nm and 1064-nm data.

The second method for determining the relative calibration of the 1064-nm and 532-nm signals can be summarised as follows:

1. The 532-nm signal is fitted and rescaled to the reference profile in a cloud-free region of the atmosphere giving a value of the calibration factor at 532 nm, C_{532}. (Here the altitude region from 17.5 km to 40 km was used.)
2. The cloud boundaries were determined using a feature-finding algorithm.
3. The effective cloud transmittance and average extinction per metre, σ_C, were calculated using the ratio of the slope coefficients of the fits above and below the cloud as described in Appendix 1. The cloud transmittance from the satellite to range r is then approximated as $T_C(0,r) = \exp[-\sigma_C(r_t - r)]$.
4. For each non-clipped 532-nm signal at range r, the following quantity was calculated:
$$(P_{532}(r)/C_{532} - T_C^2(0,r)R_{532}(r))r^2/[T_{M,O3,532}^2(0,r)T_{A,532}^2(0,r)] = \beta_C(r)T_C^2(0,r). \quad (1)$$
Here R_{532} is the reference signal at 532 nm, and T_A is the aerosol transmittance calculated from the reference profile as in Appendix 1.
5. From the 1064-nm signals at the corresponding ranges the following quantity was calculated:
$$\begin{aligned} &P_{1064}(r)r^2/T_{M,1064}^2(0,r) \\ &= C_{1064}\beta_C(r)T_C^2(0,r)T_{A,1064}^2(0,r) + C_{1064}(\beta_{M,1064}(r) + \beta_{A,1064}(r))T_C^2(0,r)T_{A,1064}^2(0,r) \end{aligned} \quad (2)$$
6. By making the assumptions that the second term in (2) is insignificant when compared with the first, and that the aerosol transmittance at 1064 nm is close to unity, a linear regression of the values calculated in (2) to those calculated in (1) yields the value of C_{1064}, a relative calibration factor for 1064 nm. In the above, P is defined as before, β is backscatter, T is transmittance, r is range, and the subscripts C, A, M and $O3$ refer, respectively to aerosol, cloud, molecular and ozone.

The results of such an analysis, applied to data from Orbit 125, are plotted in Figure A2-2 and can be compared directly with Figure A2-1. It can be seen that the uncertainties increase dramatically in regions where the cloud is thin. As expected, the values are higher than the corresponding values in Figure A2-1, but are more scattered. The higher values of the ratio seen in the higher cloud in Figure A2-1 do not seem to be reproduced in this figure, although the data are really too scattered to be certain.

The results of the more complex analysis presented in Figure A2-2 seem to be too noisy to be useful. There are two main reasons. The first is the variation from profile to profile in the calibration of the 532-nm signals against the reference signal. The second results from the fact

that many of the 532-nm signals in the regions studied for Orbit 125 were saturated, leading to too few points for good regressions. To see if better results could be obtained from signals that were not saturated, data from Orbit 013 were studied. These data were recorded during nighttime at a lower gain. As a result, no saturation occurs in any of the data channels. The disadvantage though, is that the signals are relatively weak and the SNR low, making calibration against reference profiles much noisier. Therefore the second method of analysis described above was not attempted. The simpler analysis was applied to the data and the results plotted in Figure A2-3. Points to note are the significant differences in the ratios for different clouds (compare the ratios near +10 degrees with those at –5 degrees) and the significant variation of the ratio in one cloudbank at 10 degrees latitude. This cloud bank changed altitude rapidly with latitude.

One possible reason for these inconsistent ratios could be variations in cloud particle size. To further study this possibility, the simple ratios of the 1064-nm data to the 532-nm data, corrected for calibration factors and molecular and ozone transmittances as described above, were calculated at each point in the profile. Note that, in this case, we are simply talking about ratios, whereas previously the slope coefficient of the linear regression of the 1064-nm points against the 532-nm points was used. These “colour ratios” are plotted as a function of altitude and latitude for sections of Orbits 125, 13 and 104 in Figures A2-4, A2-5 and A2-6. In Figure A2-4, the ratios in regions where the 532-nm data are saturated are blacked out.

The results show that the clouds over a large latitude range have comparable colour ratios although there does seem to be a correlation of slightly higher ratios with slightly stronger scattering with lower ratios more common near the top and bottom of the clouds in Orbit 125. However, in the results for Orbit 13, there does appear to be a slight change in the ratio with altitude and closer inspection reveals falling streaks of higher ratios. Also, ratios that are much larger than the rest of the cloud can be seen at the cloud boundaries. The reason for this is unexplained. If a slight mis-registration of the ranges of the two signals, or a slight difference in signal risetime in the two detector-amplifiers can be ruled out, then the results could be indicating a difference in the cloud particles. Note that most of the differences occur near the lower boundary of the cloud.

An interesting feature to note in Figure A2-4 is the easily detectable and slow variation with latitude of the colour ratio for the aerosol layer below 2 to 2.5 km in altitude. This obviously is related to the change in the size distribution of the aerosols, and could prove useful in selecting appropriate value of the lidar ratio in these regions.

Appendix 3: Software developed for this project

The original intention of this study was to use lidar analysis software, currently in use at CSIRO Atmospheric Research, to test various analysis algorithms on both PICASSO-CENA and LITE data. This PC-based software (`PROFILE`), written originally for the Lahey F77L, 16-bit compiler, was largely rewritten in 1994 (as `PROFIL32`) in Lahey Fortran F77L EM32, a 32-bit compiler with many Fortran 90 extensions and a DOS-extender to allow the use of extended memory. It has been developed by the author over a number of years for the analysis of lidar data from a number of sources. These include the old CSIRO ruby lidar, the newer multiwavelength scanning lidar, the minilidar, and MicroPulse Lidar (MPL) data. Various analysis algorithms and other processes can be applied to single profiles, to averages of several profiles, or to individual profiles in a set using a batch mode of analysis. Recently, the batch mode routines from `PROFIL32` have been converted to IDL for the routine analysis of MPL data from ARM CART (Atmospheric Radiation Measurement Cloud And Radiation Testbed) sites by a former colleague (R. T. Austin) and another Colorado State University scientist (C. Mitrescu).

It was soon found that the structure of the PICASSO-CENA data was far too incompatible with the other lidar data formats to allow the use of the existing software. The changes to the existing software necessary to allow the use analysis of the PICASSO-CENA data were so extensive that it was decided to write a new program and incorporate only those routines from `PROFIL32`, in a significantly-modified form, which were needed for the analysis of individual, averaged profiles. Additional, pre-processing software was written to allow the raw PICASSO-CENA data to be read and saved as averages of a number (1, 2, 5, 10, 20, ...400) of individual profiles. This software also extracted the reference molecular profiles required in the subsequent analysis.

Again, when the LITE data were received, it was found that the data structure, although more compatible with the ground-based data format, still required substantial changes to `PROFIL32`, mainly because the ground-based data associate increasing range with increasing altitude. The opposite situation with the space lidar data would have required many changes, particularly to the cloud base and top detection software. The LITE data were also quite different from the PICASSO-CENA data, being organised in 1500-shot “granules” covering some two minutes of orbit, whereas the latter data set were composite profiles with both resolution and averaging scheme varying with altitude. The LITE data were also in binary files and several bit-swapping routines had to be written to allow their use with the author’s PC-based software. Therefore, another set of routines was written for analysing the LITE data. This incorporated significantly-modified, batch processing routines from `PROFIL32`. The various routines are summarised below.

`PLOTPICS.F`

This is a modification and extension of an IDL program, written by Kathy Powell of NASA LaRC, for the display of PICASSO-CENA data, and available for download on the PICASSO-CENA simulation website. The very large number of variables employed in modelling the lidar signal, the very long variable names, and other characteristics of the software led to the decision to write a program incorporating large sections of the IDL program converted to free-source Lahey F77L EM32, this compiler allowing the use of allocatable arrays and other features used extensively throughout the IDL code. (A conversion to FORTRAN 90 would have been simpler, but the author was not adequately set up for FORTRAN 90 at the time.) The sections of the code ported from IDL carried out the complicated process of reading the simulated data files and reconstructing lidar profiles from the complex (but space-saving) format in which they are stored. The remainder of the

program created output files of the molecular reference profiles and averages of a selectable number of individual profiles.

The program can use the long filenames in the original data, e.g. sim_0034_p_001. The simulated data files are in simple, ASCII format.

ANALPICS.FOR
This program, written in Lahey F77l EM32, displays the PICASSO-CENA profile being analysed, and incorporates routines from PROFIL32 for the analysis of individual, averaged profiles using a number of different algorithms. The selection of the many variables during the processing is via menus, the software libraries for which were written by Denis O'Brien of CSIRO Atmospheric Research.

LITEREAD.FOR
LITE data from a data granule containing 1200 profiles can be read and viewed rapidly (10 - 20 profiles per second) to allow the initial selection of analysis parameters, data windows containing cloud, clear regions or boundary-layer aerosols. Latitude, longitude and time (UTC) are also displayed and the process can be paused to allow these values to be read and subsets of the granule selected for particular attention.

The program is written in Lahey F77L EM32. LITEREAD (and LITEANAL described below) cannot use the long filenames in the original data. Data files have been saved with shorter names to allow use with this software in a PC environment (DOS environments, or DOS windows under MS Windows 3.1 or 9x, or IBM OS/2). For example, a two-minute data granule of level 1 data from LITE Orbit 125, starting 16:12:08 UTC on 17th September 1994, with the original name LITE_L1_19940917_161208_161408 has been saved as L1161208.125.

SATANAL.FOR
This program is also written in Lahey F77L EM32, and incorporates the batch and single-profile average analysis routines from PROFIL32. Data can be displayed in various ways, averaged, smoothed, calibrated, analysed and so on. Many different forms of output files can be produced, allowing for the display of the results of the analysis of single profiles, or a collection of contiguous data granules, which can be displayed with the accompanying time versus height plotting software.

A method has been devised for the creation of running averages of a (user selectable) number of profiles. The LITE scenes can thus be smoothed in time as well as in height. This is a very useful facility, as it allows for the comparison of the results of "retrieve then average" as opposed to "average then retrieve" analyses. This is an issue receiving considerable attention by the developers of the PICASSO-CENA ATBD.

The various capabilities of the program are summarised below:

1. Raw or scaled profile data can be displayed, one channel at a time, or all three simultaneously.
2. Profiles from a scene can be averaged then, saved as an output file, fitted to a reference profile, analysed and saved. Reference, cloud-free, profiles can be produced.
3. Previously-saved average profile files can be read in for further processing.
4. Profiles in a scene can be fitted to either a reference or an average profile, and output files containing the fitting parameters and also height versus latitude values of the ratio of the profile to the average can be produced.

5. Profiles in a scene can be analysed using a variety of algorithms and output files containing the calibration data and cloud base and top, optical thickness and lidar ratio and other data produced. Files containing values of extinction or backscatter as a function of latitude and height are also produced and can be displayed with associated routines.
6. The variation of the calibration between 1064-nm and 532-nm data can be studied an output files produced.
7. Files for the display against time and height of the variation of the ratio of the signal at 1064 nm to that at 532 nm can be produced.

HVLAVE.FOR

The output files produced in option 5 of SATANAL above are read and averaged, and statistics and an output profile file produced.

This provides the other part of the "retrieve then average" versus "average then retrieve" facility described above.

HVLPLOT.FOR

This is the routine that allows the display of the data files produced in SATANAL options 4, 5, and 7 above, in colour diagrams with the variable plotted as a function of height versus latitude. The program is a minor modification of the routine HVTPLOT that was written some years ago for the display of similar data files produced by PROFIL32 for ground-based lidar data. Unfortunately, the graphics software is no longer available and will only run on PCs incorporating a limited range of graphics cards. However, the input data files are of a fairly simple ASCII form and IDL software has been written by R. Austin for the display of these files.

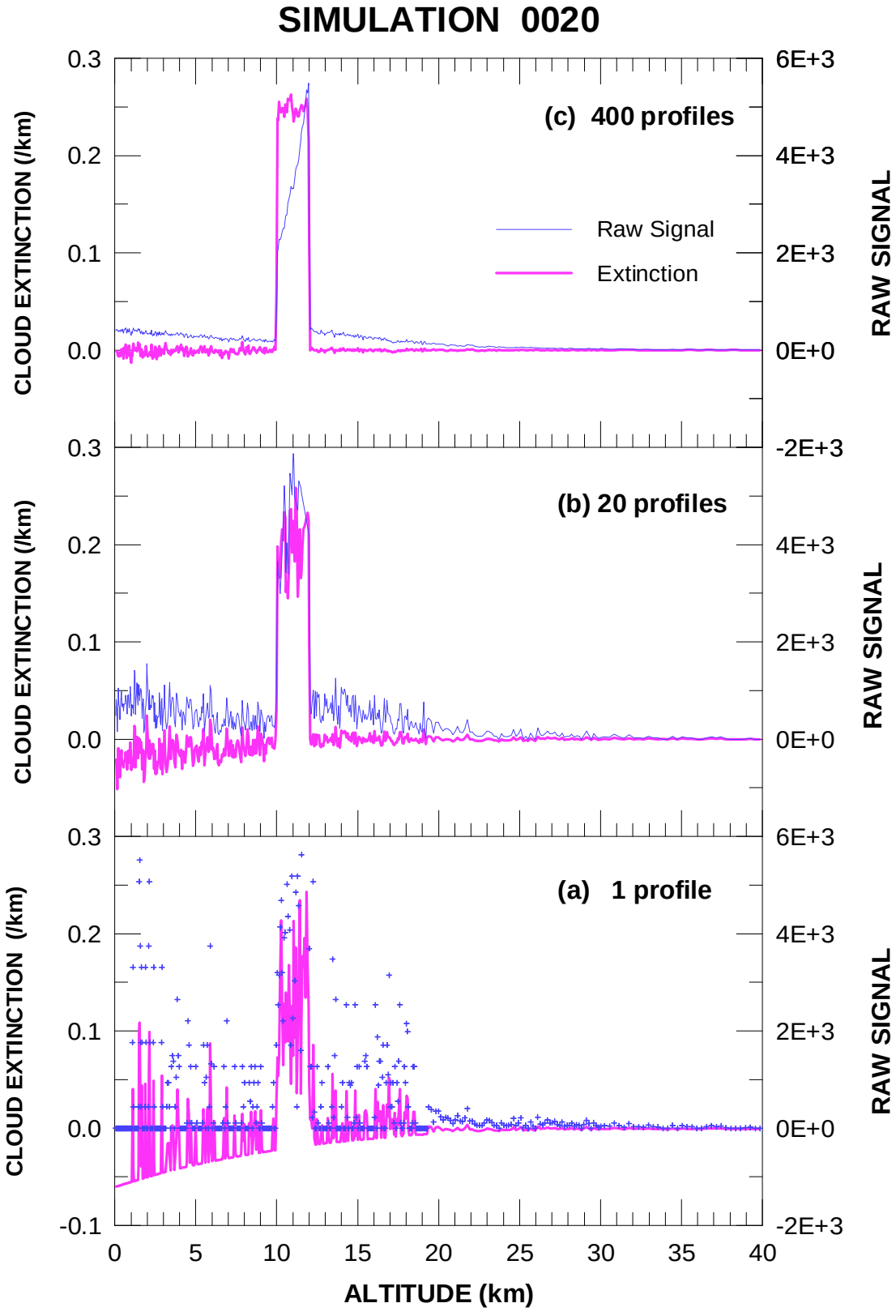

Figure 1. Simulated PICASSO-CENA data plotted as the fine (blue) lines or + symbols in (a), and the retrieved profiles of extinction as the heavier (magenta) lines. . The simulated extinction was 0.25 km^{-1}, optical thickness 0.5 and lidar ratio, S_c, 44.3 sr. The panels show the results of averaging the following number of profiles (a) 1, (b) 20, (c) 400.

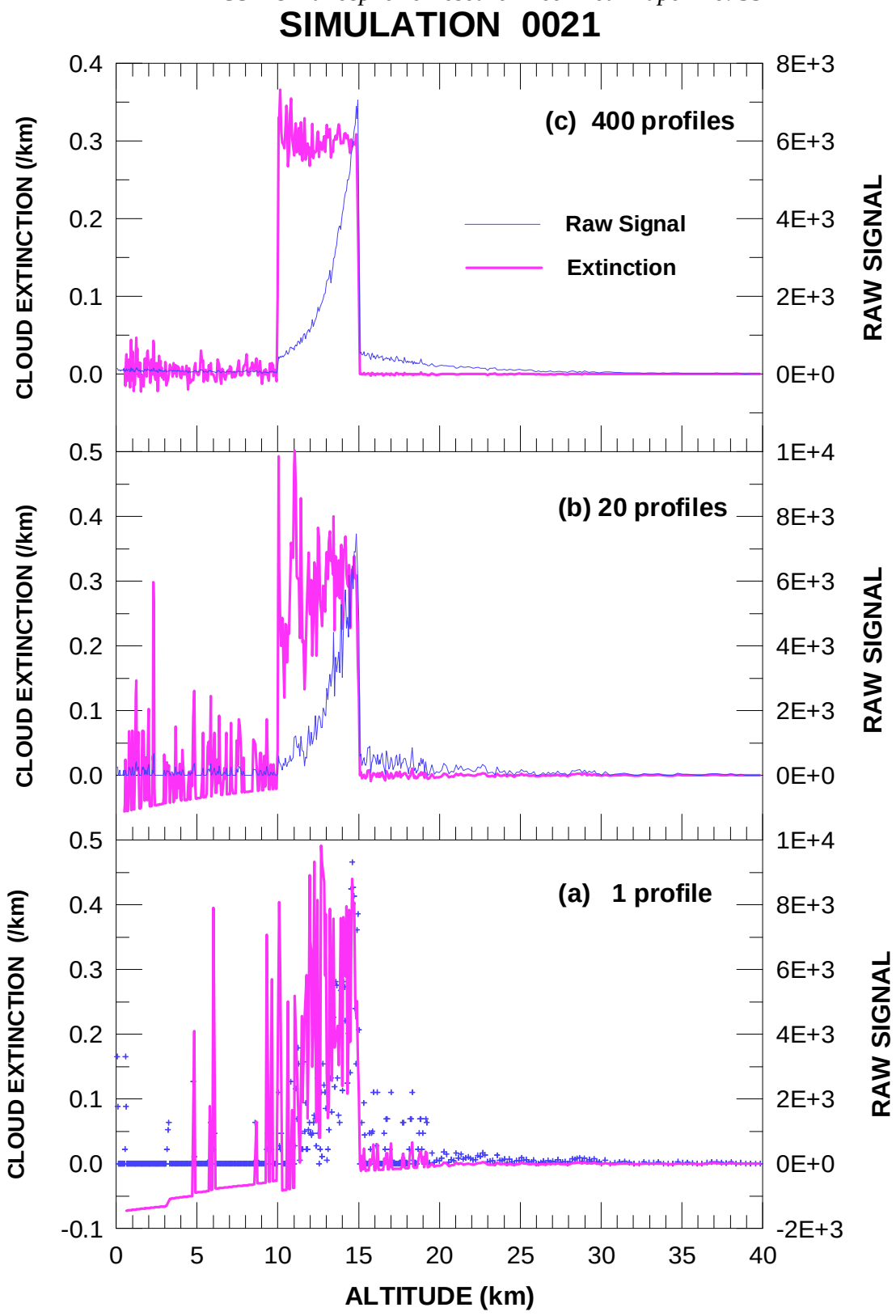

Figure 2. Simulated PICASSO-CENA data plotted as the fine (blue) lines or + symbols in (a), and the retrieved profiles of extinction as the heavier (magenta) lines. The simulated extinction was 0.30 km^{-1}, optical thickness 1.5 and lidar ratio, S_c, 59.5 sr. The panels show the results of averaging the following number of profiles (a) 1, (b) 20, (c) 400.

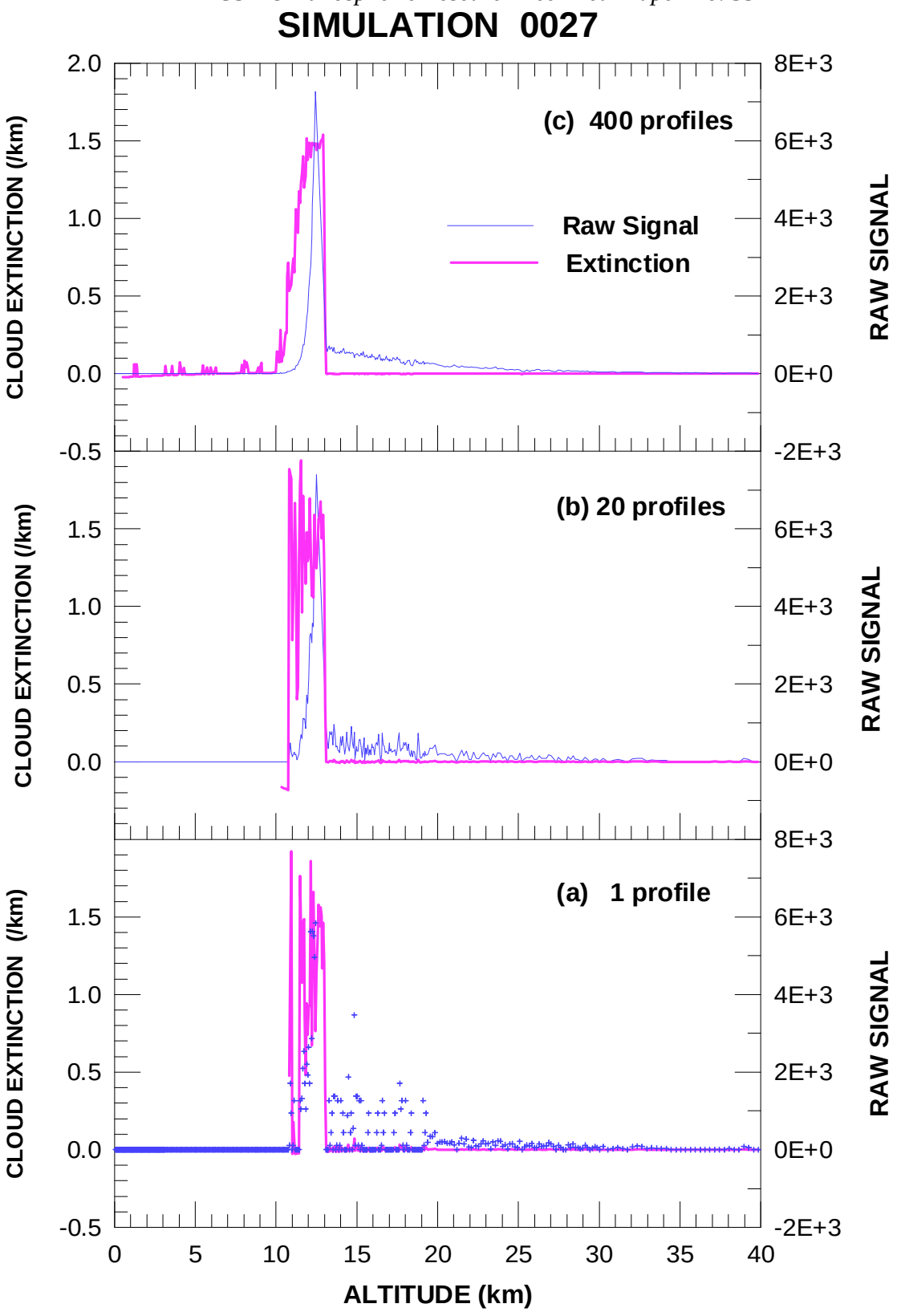

Figure 3. Simulated PICASSO-CENA data plotted as the fine (blue) lines or + symbols in (a), and the retrieved profiles of extinction as the heavier (magenta) lines. . The simulated extinction was 1.5 km^{-1}, optical thickness 4.5 and lidar ratio, S_c, 50.34 sr. The panels show the results of averaging the following number of profiles (a) 1, (b) 20, (c) 400.

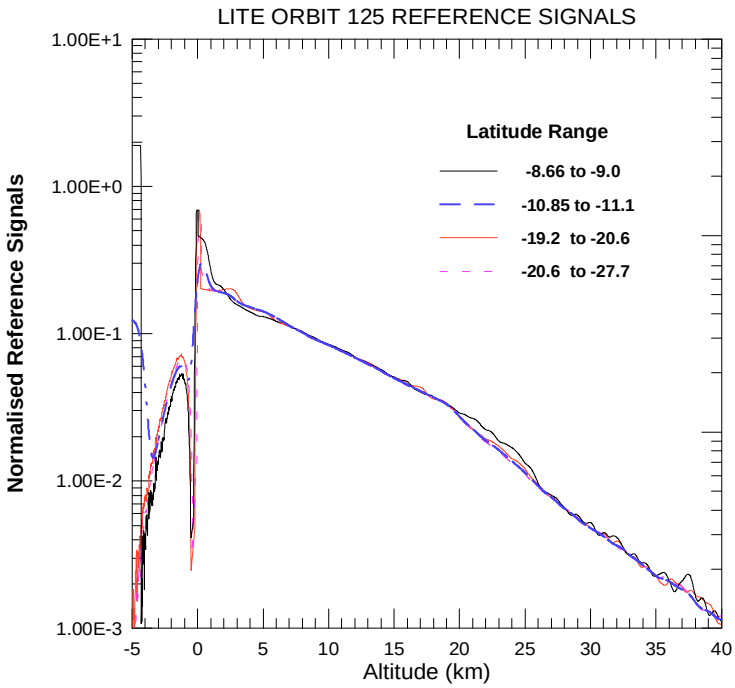

Figure 4(a). Cloud-free reference profiles used in the analysis of LITE data. The latitude ranges from which they were obtained are shown.

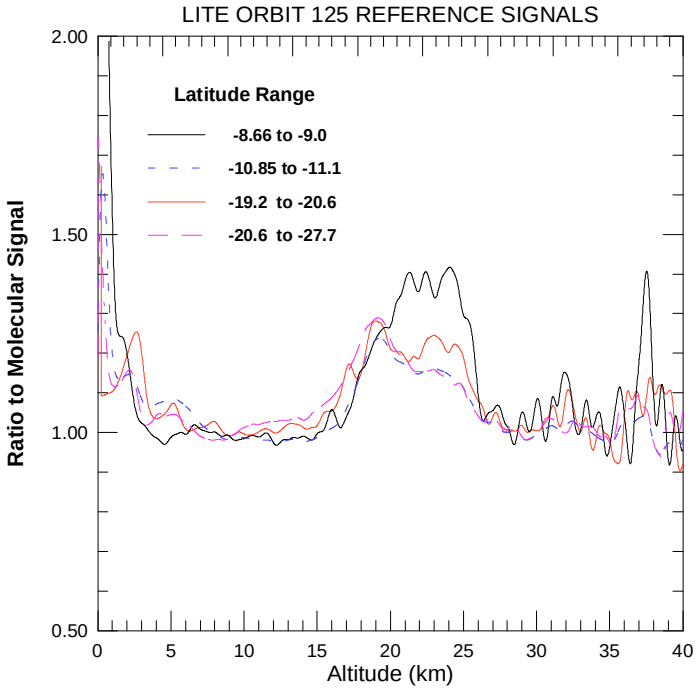

Figure 4(b) Reference profiles plotted as ratios to a molecular signal. The plots are equivalent to attenuated scattering ratios.

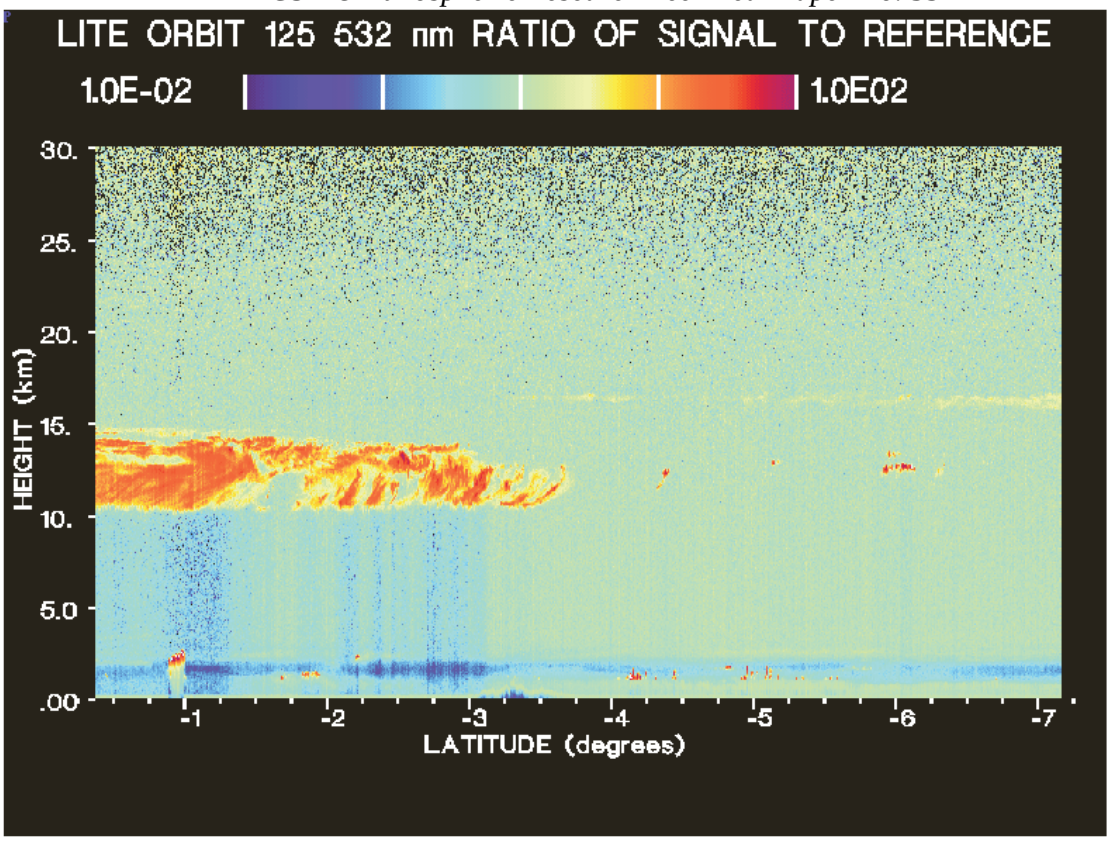

Figure 5. Ratio of each signal to the reference signal. The logarithmic colour scale covers the range 0.01 to 100. The white bars indicate decades. See text for details.

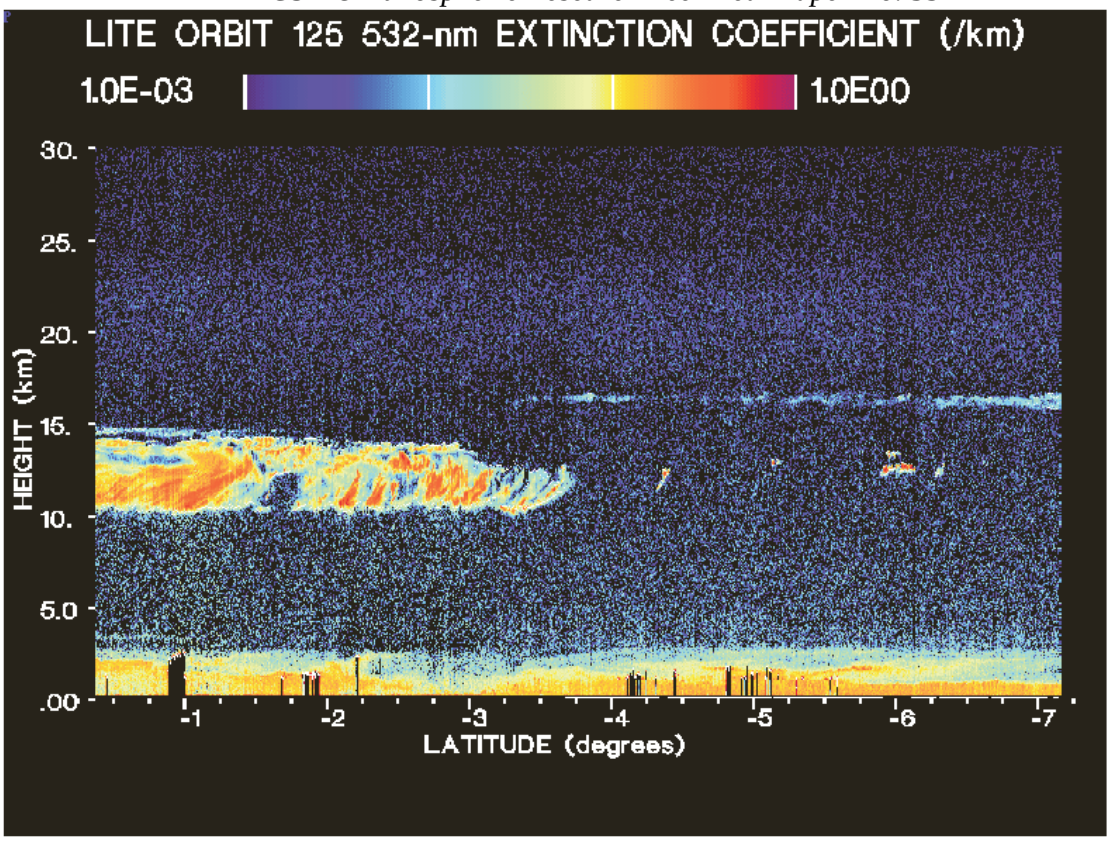

Figure 6. Retrieved cloud and aerosol extinction at 532 nm. The logarithmic colour scale covers the range 0.001 km^{-1} to 1.0 km^{-1}. No vertical or horizontal smoothing has been used. 1064-nm data have been used to replace saturated 532-nm data in clouds. Black regions below about 2.5 km indicate regions where the signal was saturated and the solution has diverged. See text.

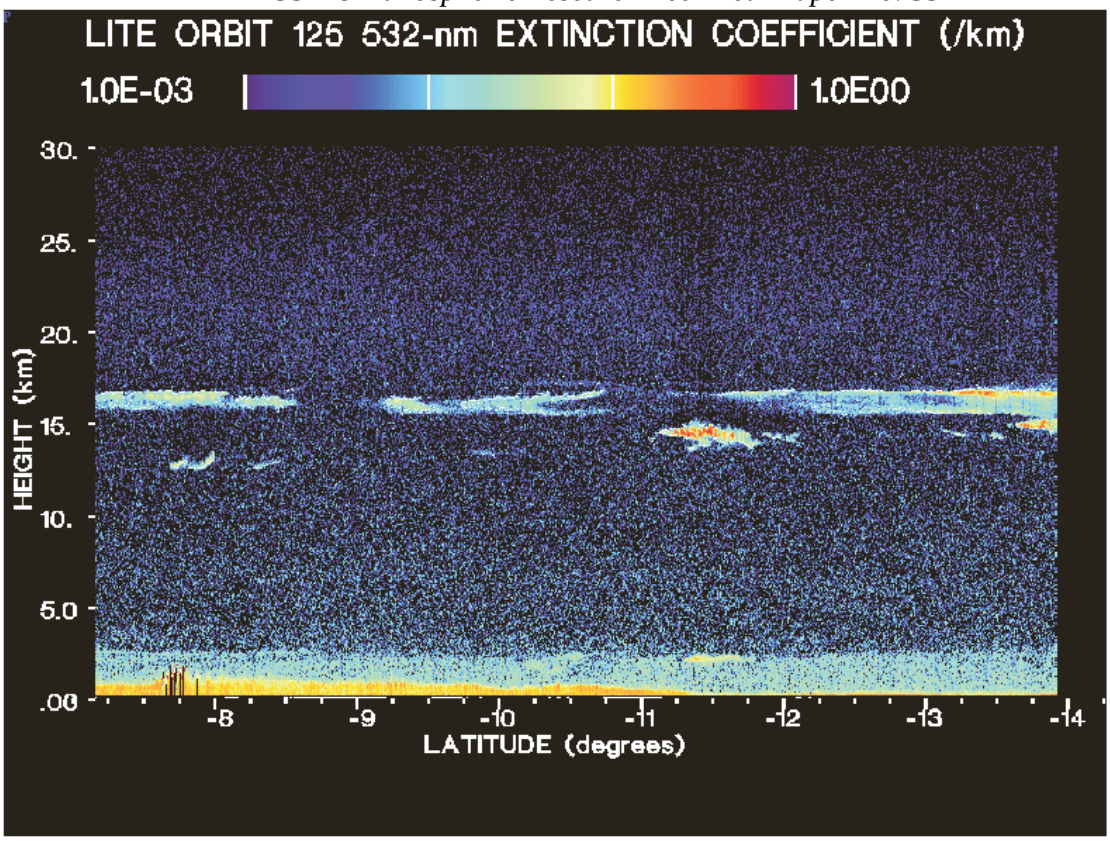

Figure 7. Retrieved cloud and aerosol extinction at 532 nm. No vertical or horizontal smoothing has been used. 1064-nm data have been used to replace saturated 532-nm data in clouds. A constant lidar ratio of 30 sr has been used in the cloudy regions. A lidar ratio of 40 sr was used for the aerosols above the boundary layer and a value of 20 sr was used for aerosols in that layer.

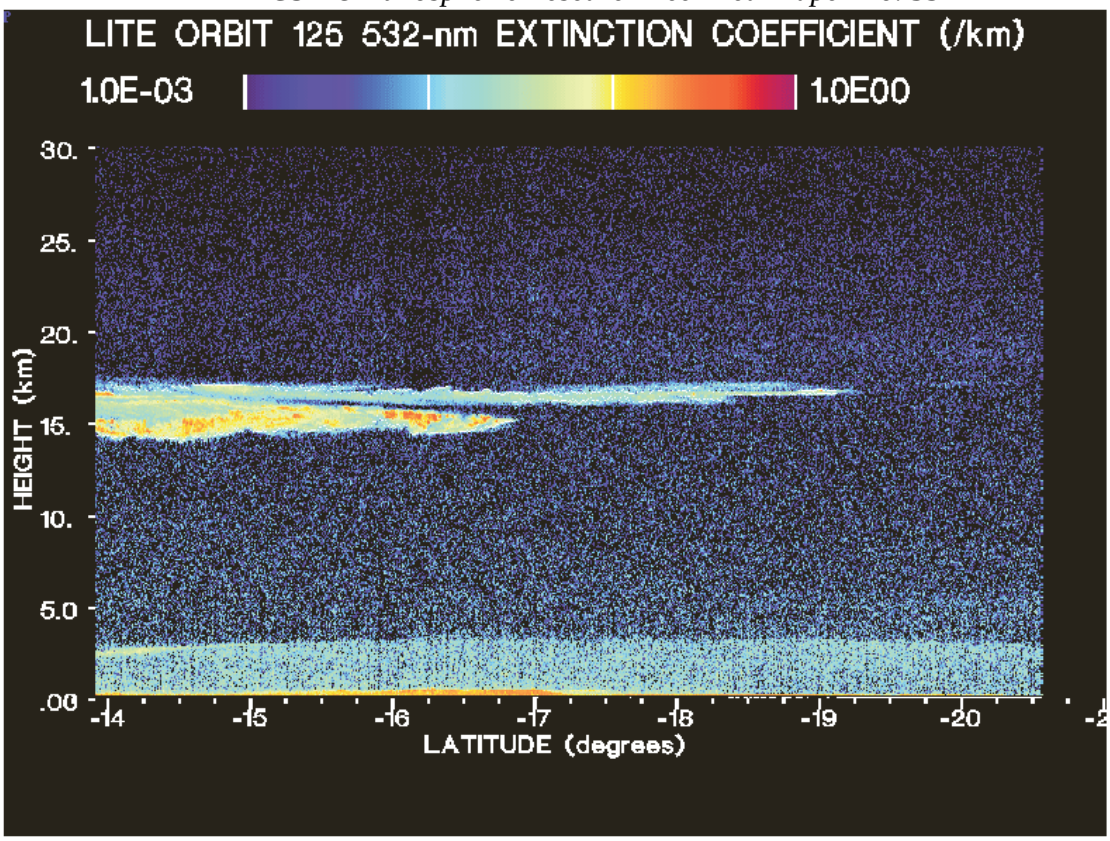

Figure 8. Retrieved cloud and aerosol extinction at 532 nm. No vertical or horizontal smoothing has been used. 1064-nm data have been used to replace saturated 532-nm data in clouds. A constant lidar ratio of 30 sr has been used in the cloudy regions. A lidar ratio of 40 sr was used for the aerosols above the boundary layer and a value of 20 sr was used for aerosols in that layer.

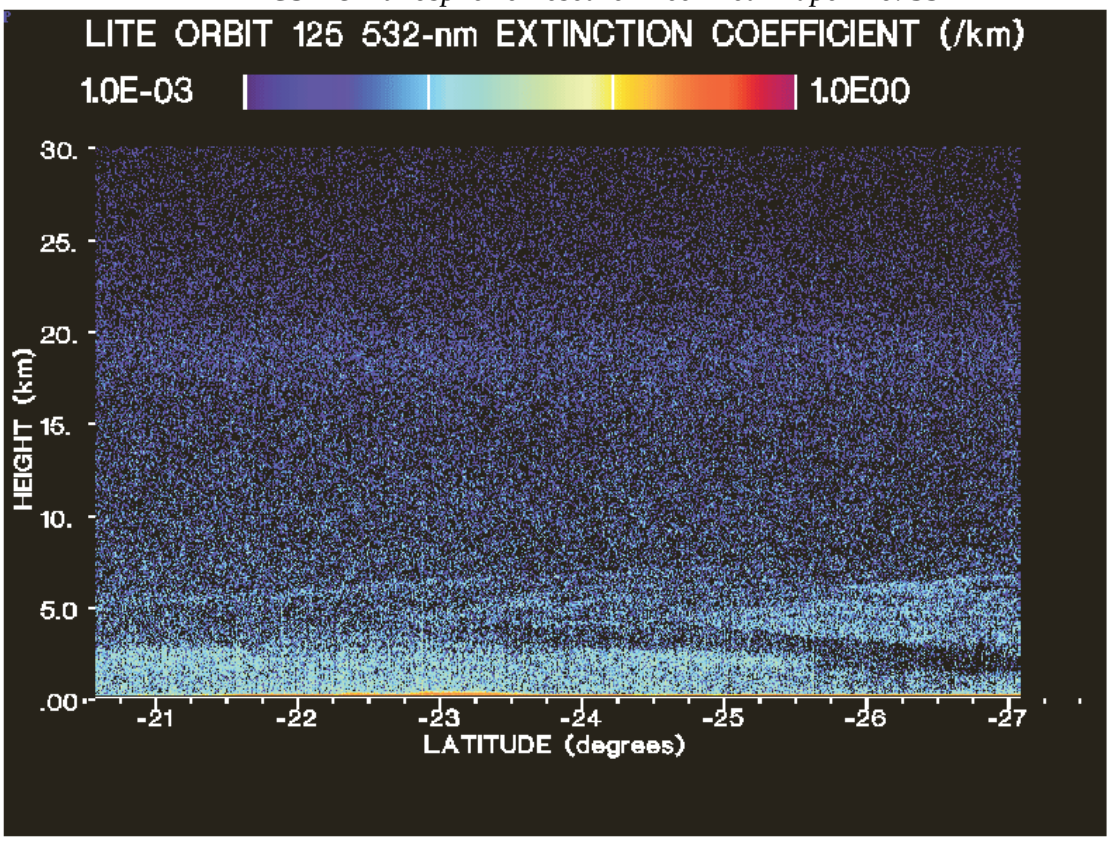

Figure 9. Retrieved cloud and aerosol extinction at 532 nm. No vertical or horizontal smoothing has been used. A lidar ratio of 40 sr was used for the aerosols above the boundary layer and a value of 20 sr was used for aerosols in that layer.

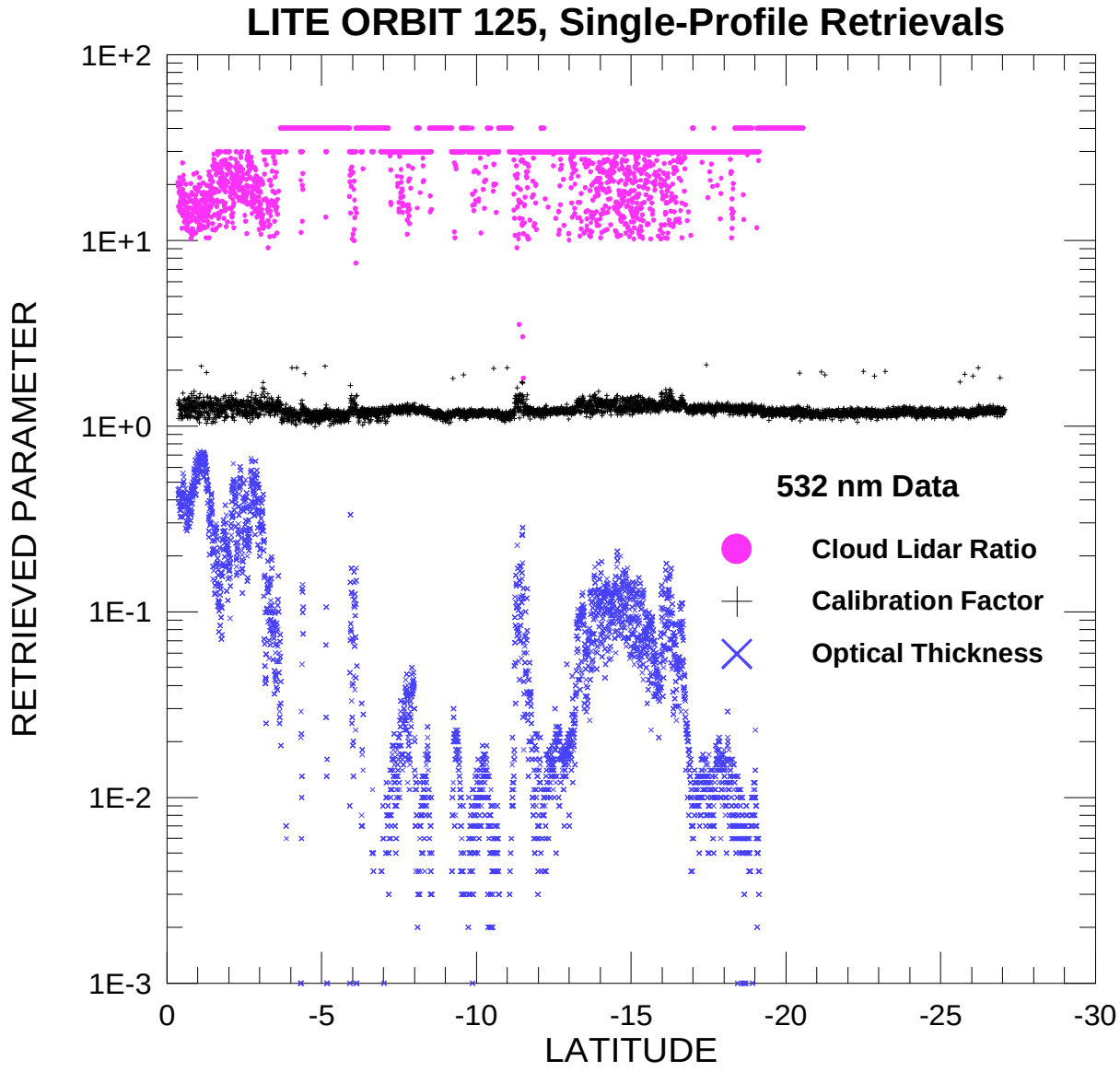

Figure 10. Retrieved calibration factors and effective optical thickness and lidar ratio for clouds detected in Figures 6 to 9.

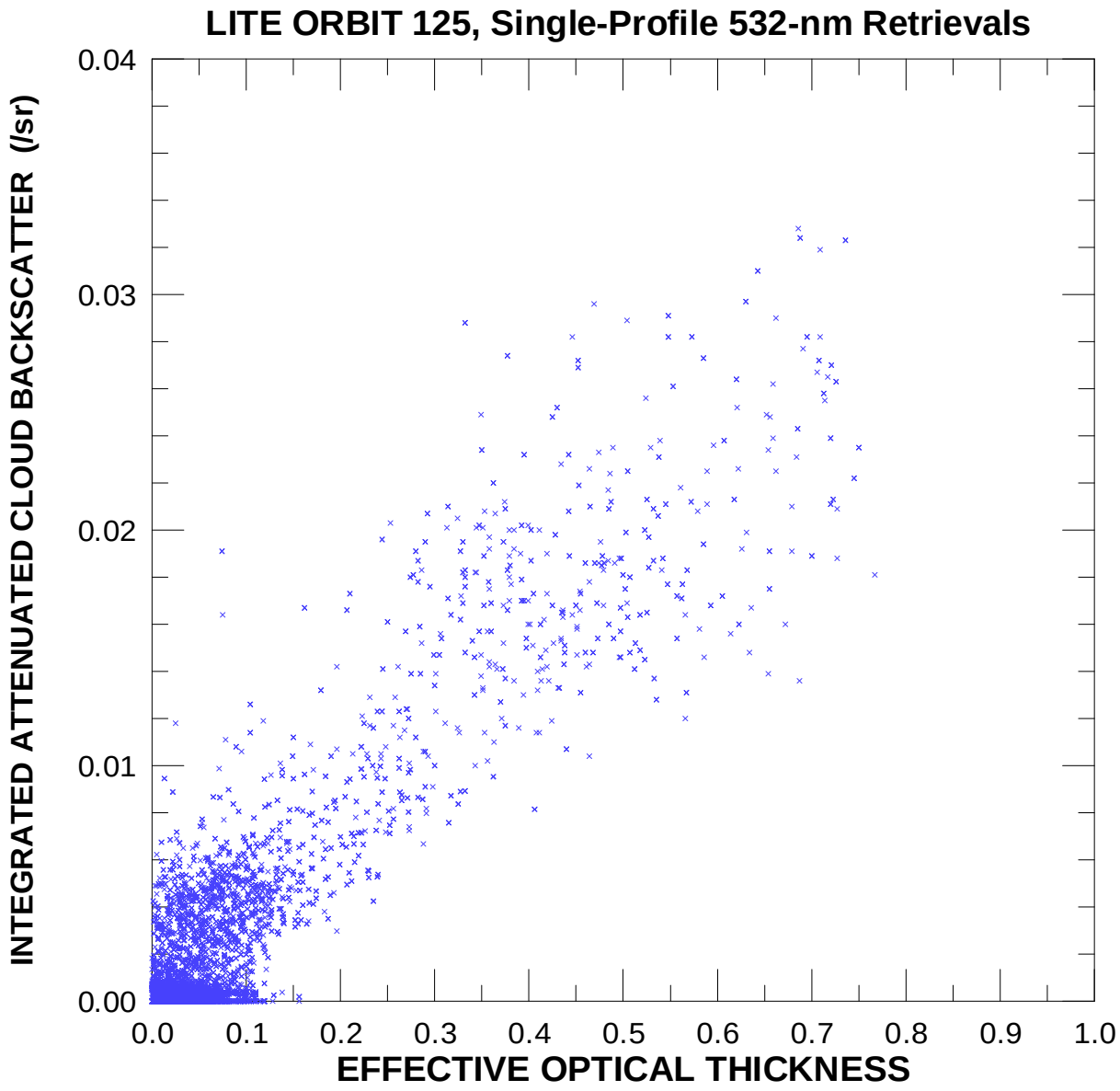

Figure 11. Integrated, attenuated cloud backscatter, $\gamma'_C(\pi)$, plotted against effective optical thickness.

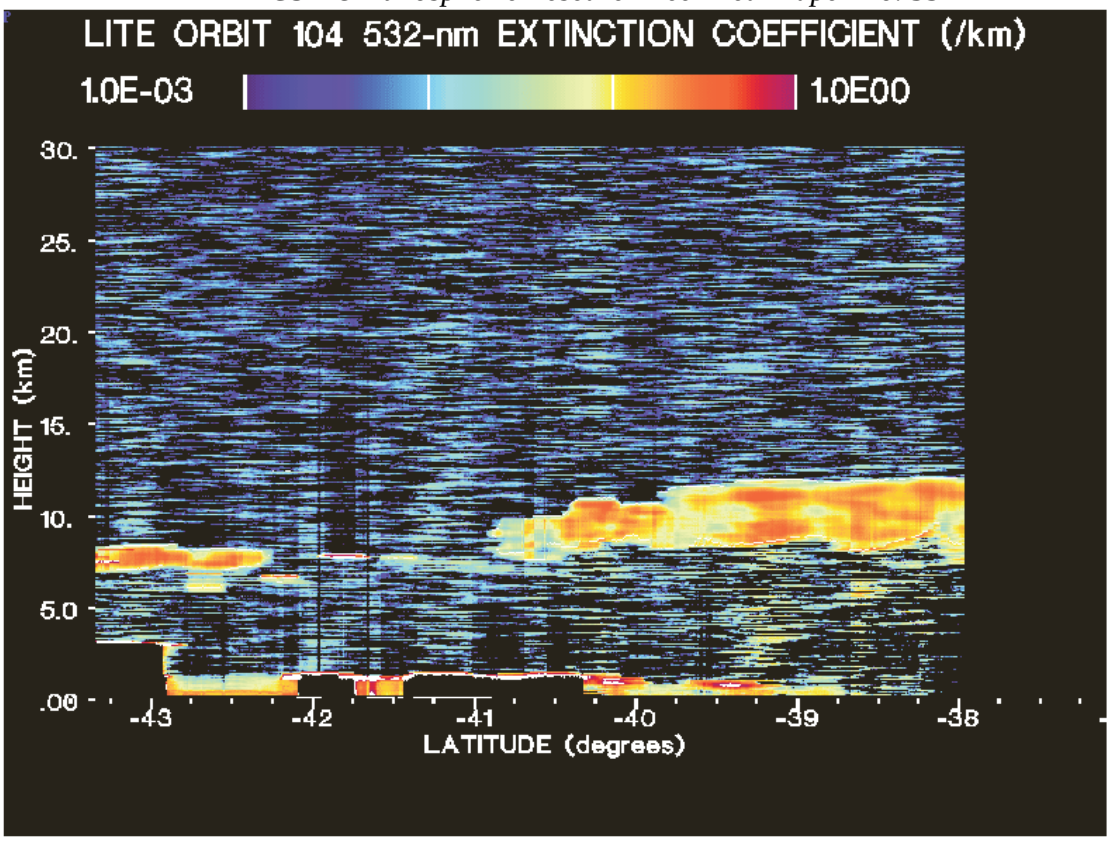

Figure 12. Retrieved cloud and aerosol extinction at 532 nm. A running mean of 50 consecutive profiles was used to increase the SNR. A lidar ratio of 40 sr was used for the aerosols above the boundary layer and a value of 20 sr was used for aerosols in that layer.

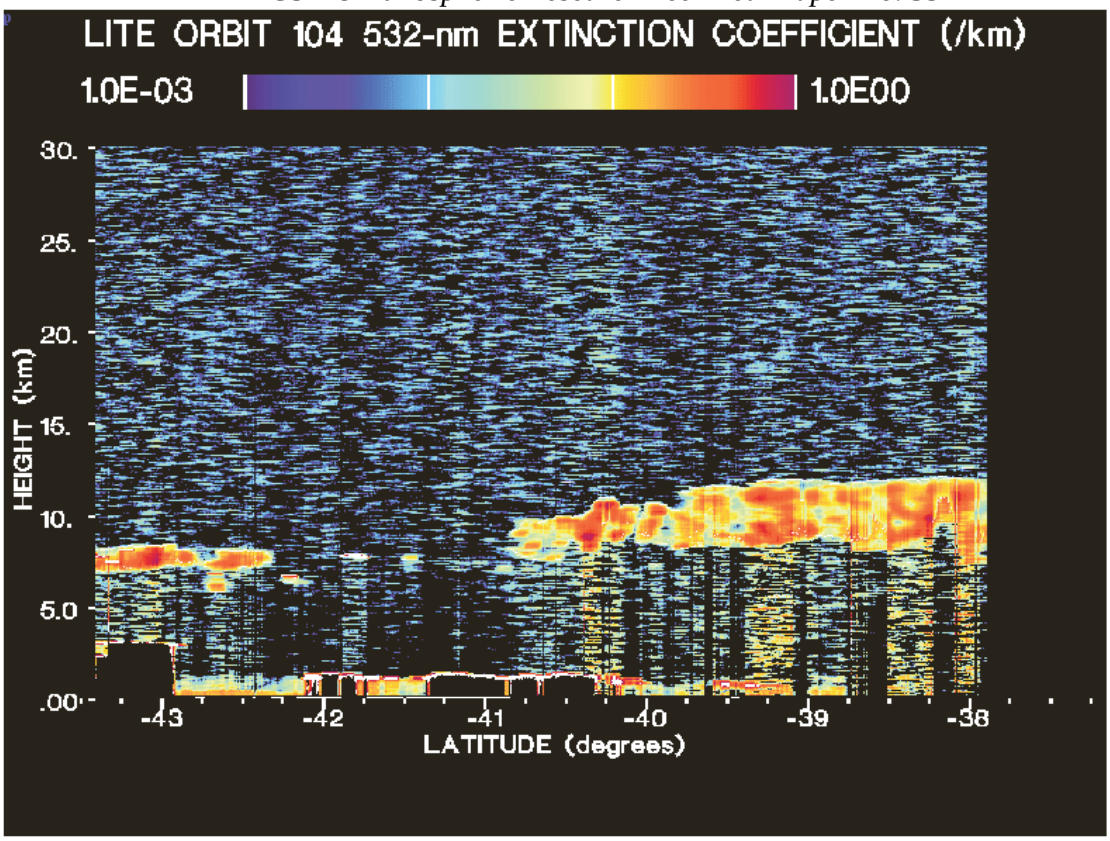

Figure 13. Retrieved cloud and aerosol extinction at 532 nm. A running mean of 20 consecutive profiles and a vertical smoothing window of 7 points (105 m) were used to increase the SNR. A calibration factor was specified and a default lidar ratio of 30 sr was set for the clouds. A lidar ratio of 40 sr was used for the aerosols above the boundary layer and a value of 20 sr was used for aerosols in that layer.

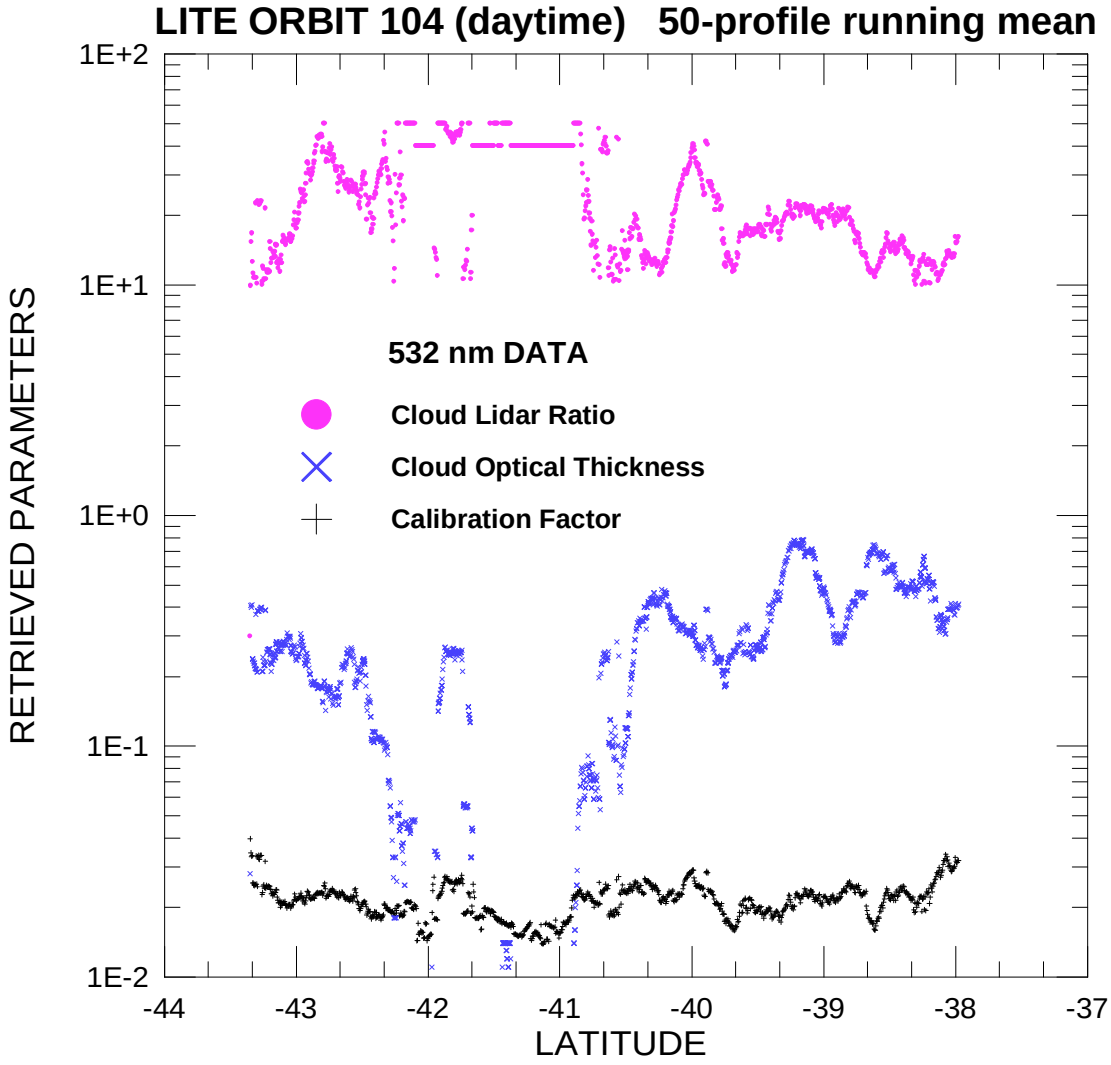

Figure 14. Retrieved calibration factors and effective optical thickness and lidar ratio for clouds detected in Figure 12.

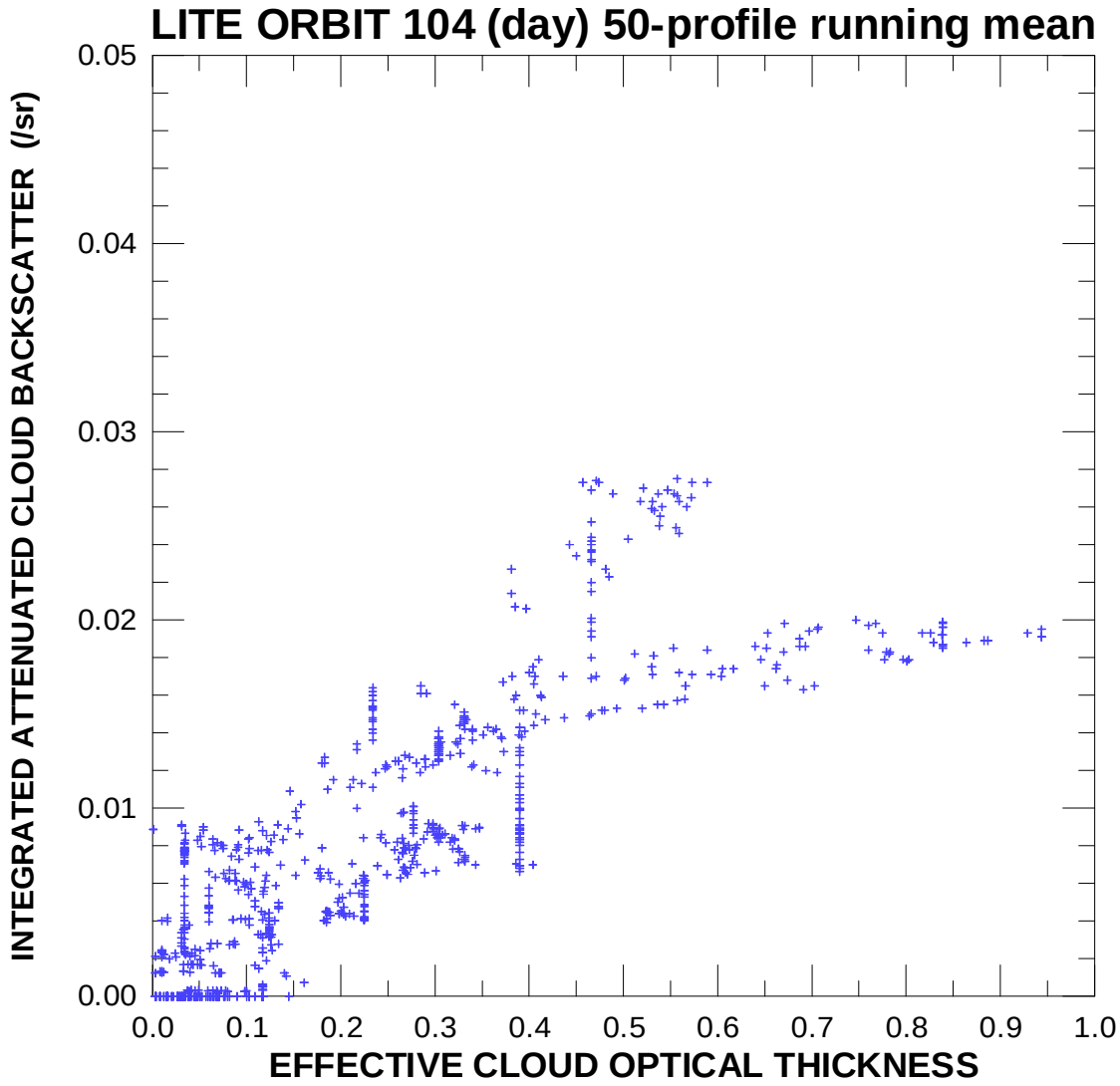

Figure 15. Integrated, attenuated cloud backscatter, $\gamma'_C(\pi)$, plotted against effective optical thickness.

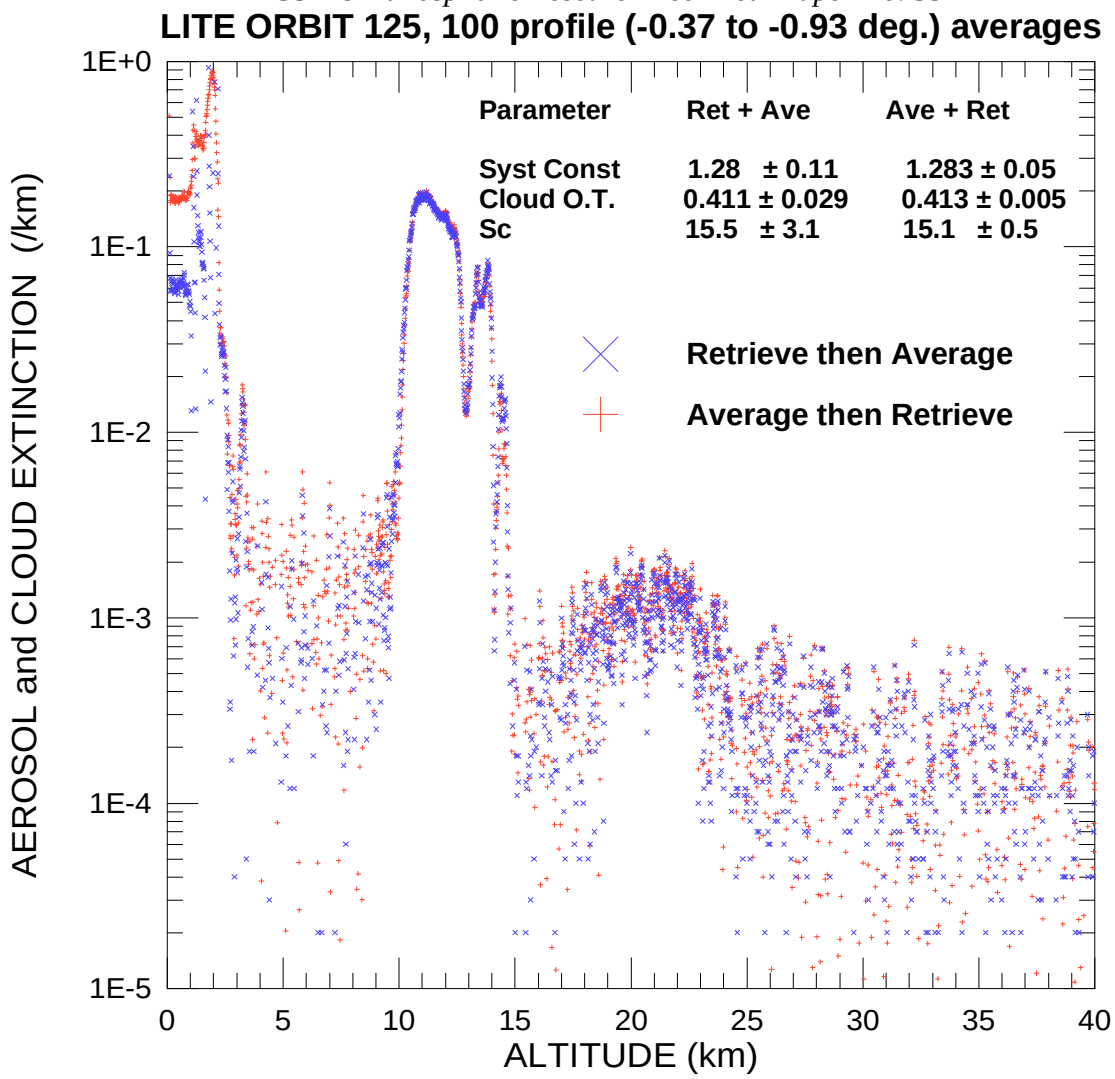

Figure 16. Comparison of "retrieve then average" with "average then retrieve" calculations of the average extinction profile for LITE Orbit 125, over the latitude range –0.366 to –0.927 degrees. The lidar system (calibration) constant (Syst Const), effective optical thickness (Cloud O.T.) and effective lidar ratio (Sc) for the cloud layer as determined by the two methods is also shown. Note that, in the text, the effective lidar ratio is represented by the symbol ηS_C.

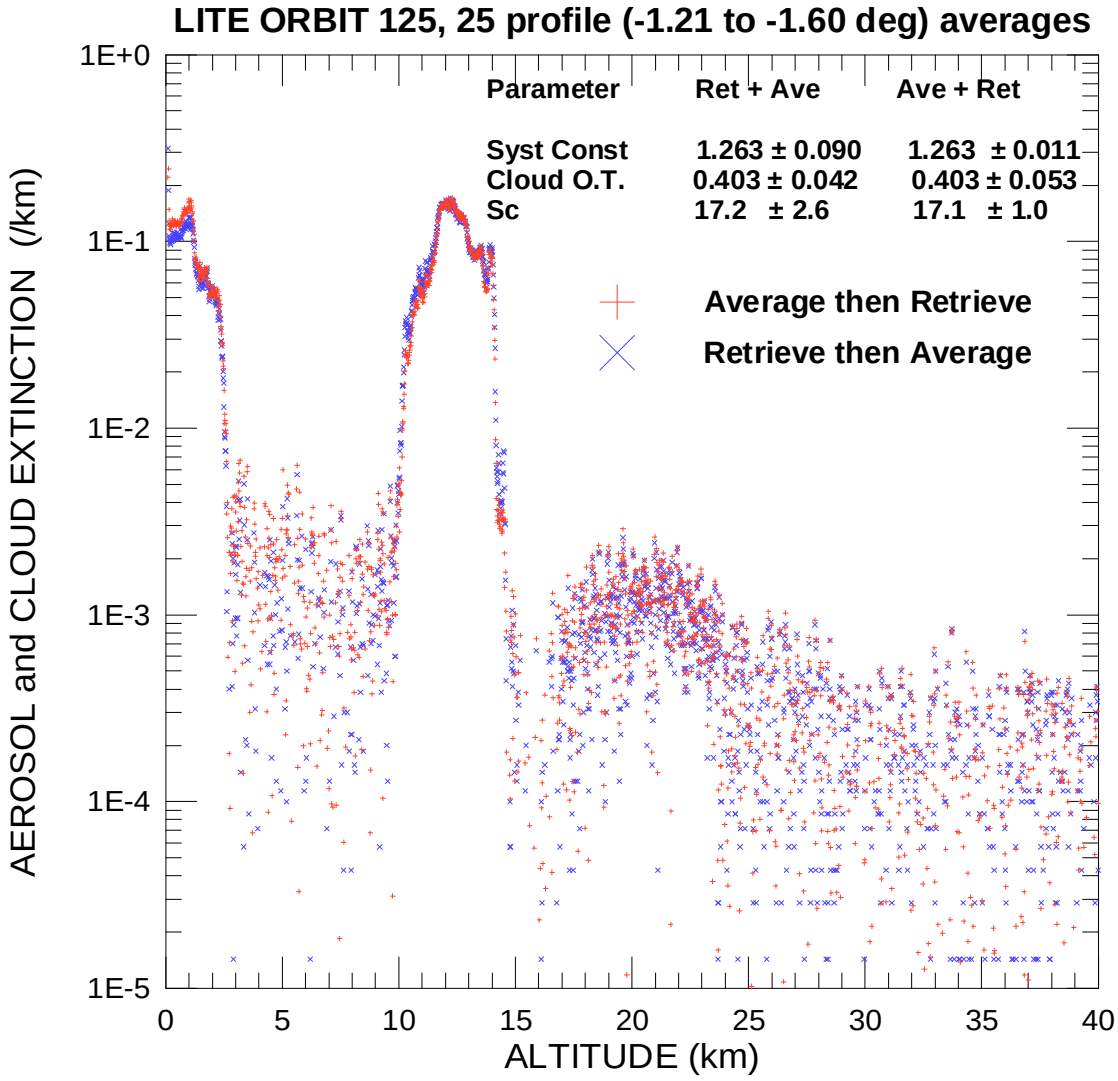

Figure 17. Comparison of "retrieve then average" with "average then retrieve" calculations of the average extinction profile for LITE Orbit 125, over the latitude range –1.205 to –1.596 degrees.

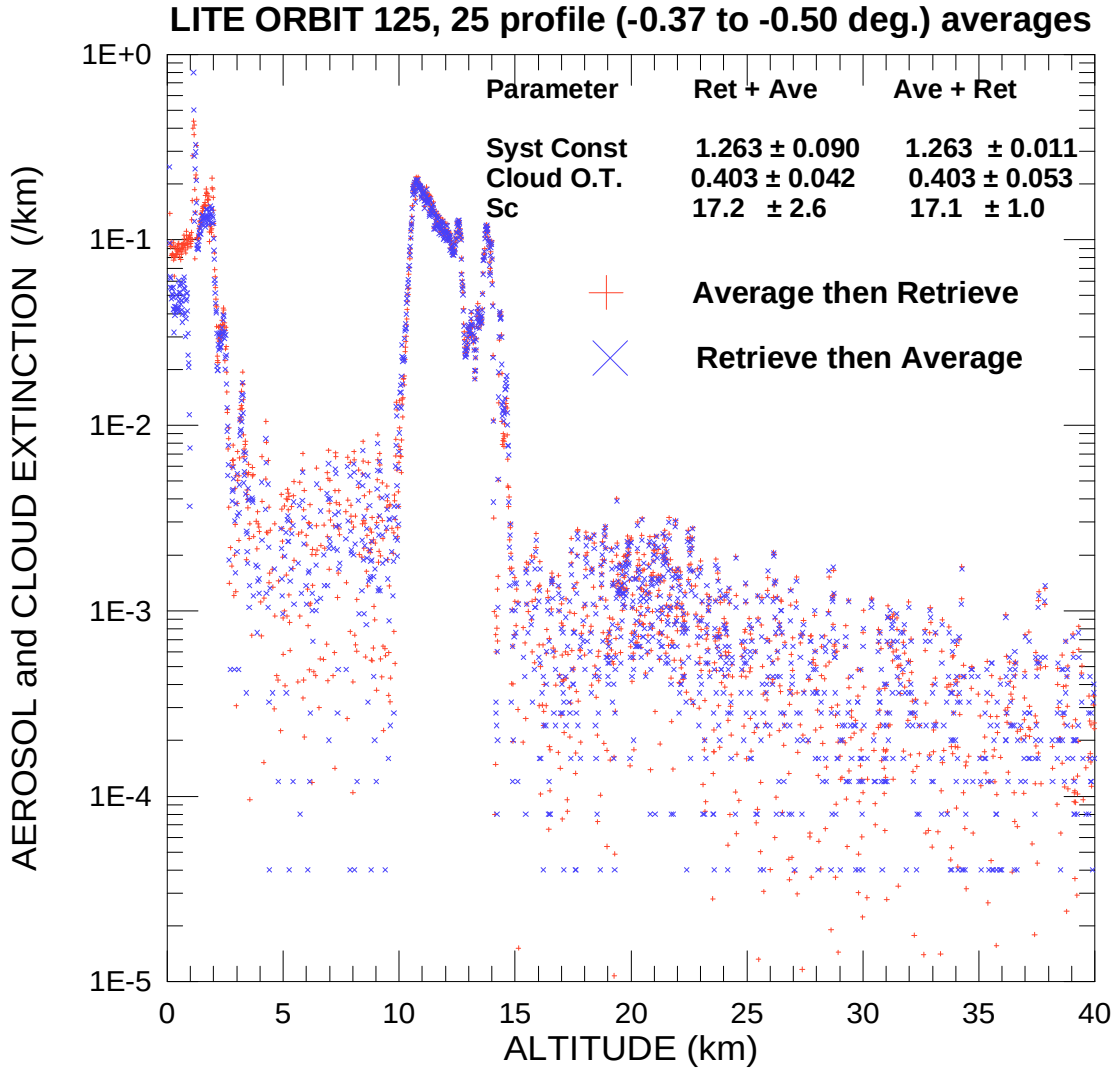

Figure 18. Comparison of "retrieve then average" with "average then retrieve" calculations of the average extinction profile for LITE Orbit 125, over the latitude range –0.366 to –0.503 degrees.

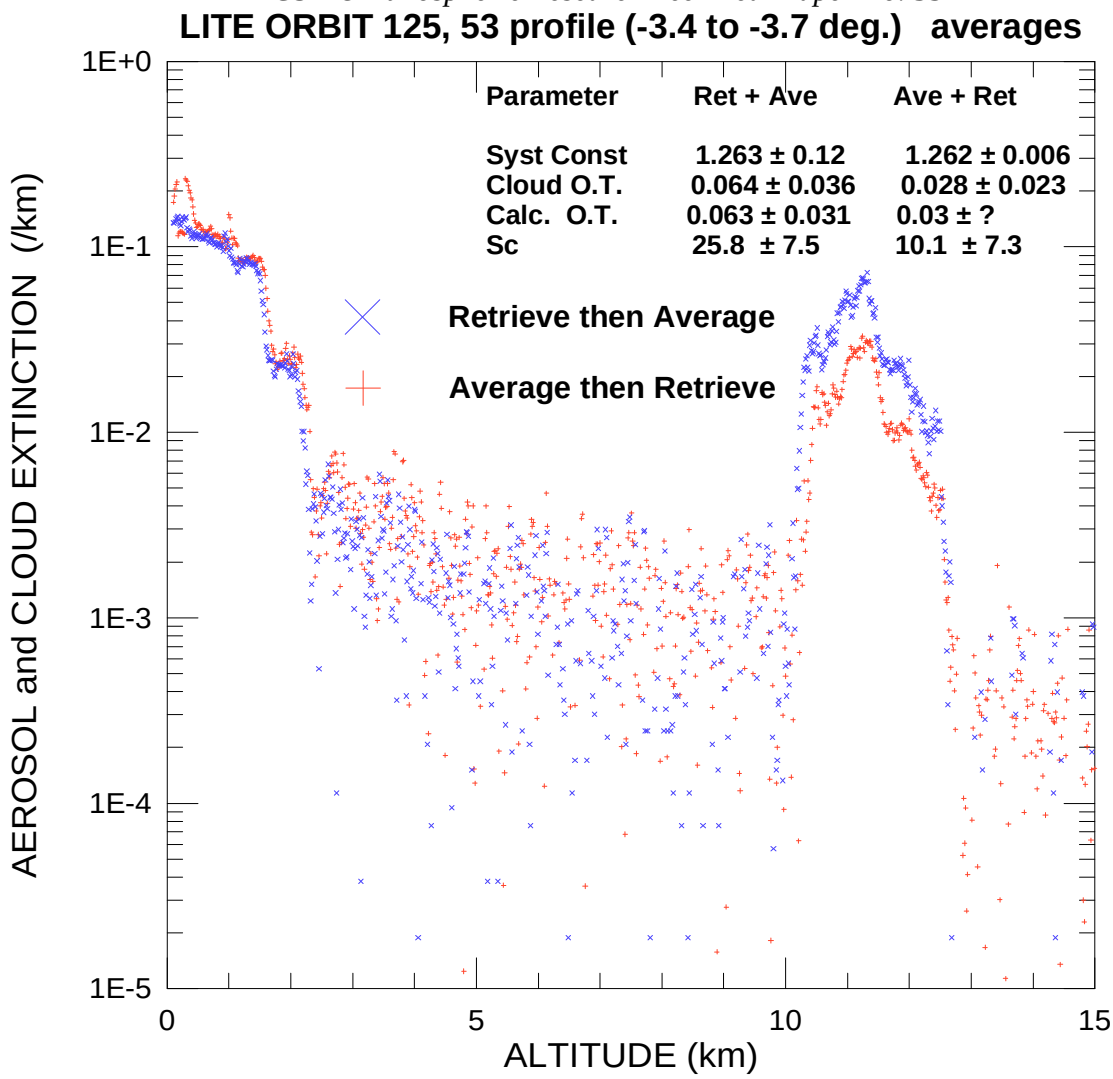

Figure 19. Comparison of "retrieve then average" with "average then retrieve" calculations of the average extinction profile for LITE Orbit 125, over the latitude range –3.402 to –3.690 degrees. The parameter (Calc O.T.) is the cloud optical thickness calculated from the integral of the extinction solution (the uncertainty is unknown), whereas the Cloud O.T. is the effective optical thickness as calculated by the method in Appendix 1. The other parameters are defined in Figure16.

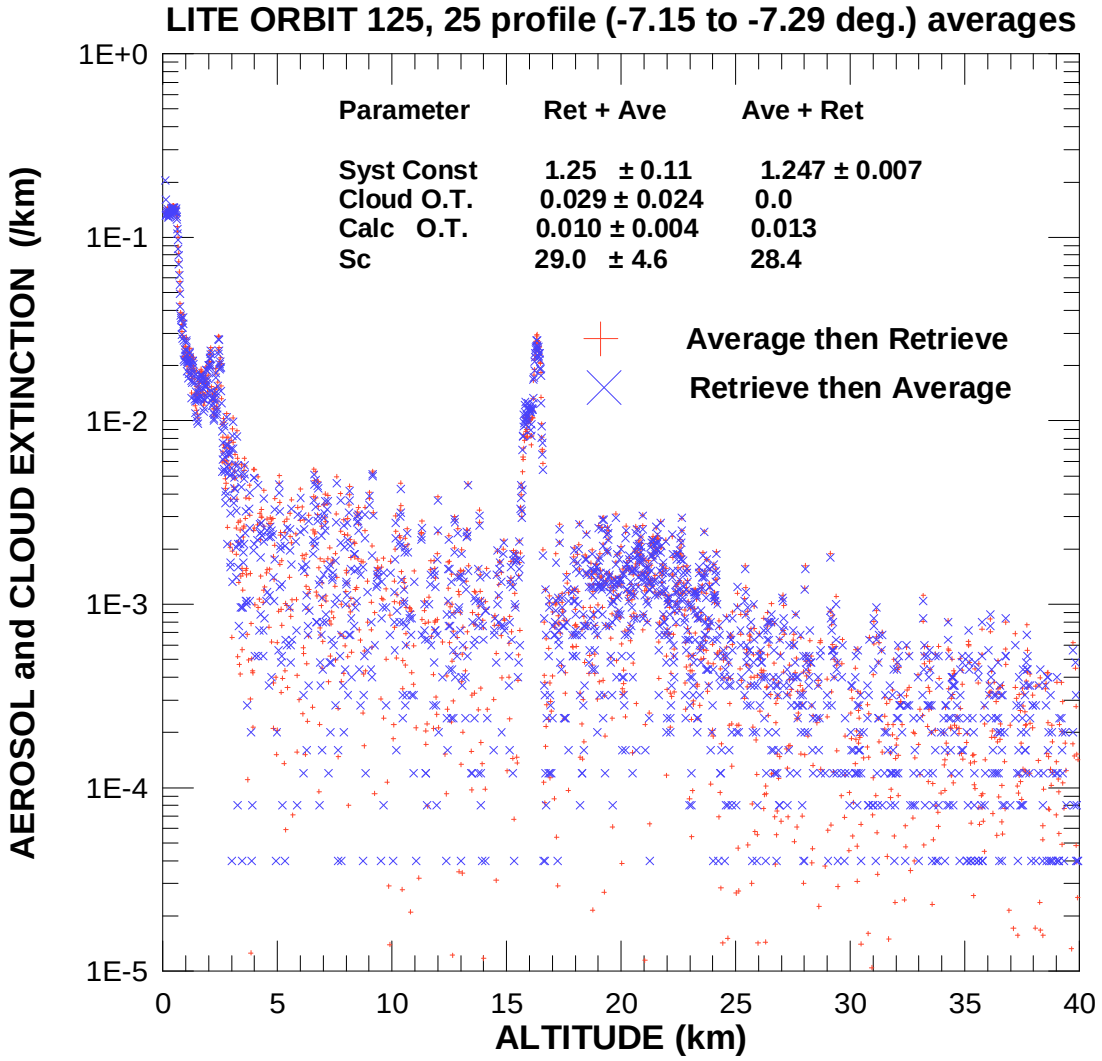

Figure 20. Comparison of "retrieve then average" with "average then retrieve" calculations of the average extinction profile for LITE Orbit 125, over the latitude range –7.153 to –7.288 degrees. The parameter (Calc O.T.) is the cloud optical thickness calculated from the integral of the extinction solution, whereas the Cloud O.T. is the effective optical thickness as calculated by the method in Appendix 1. The other parameters are defined in Figure16.

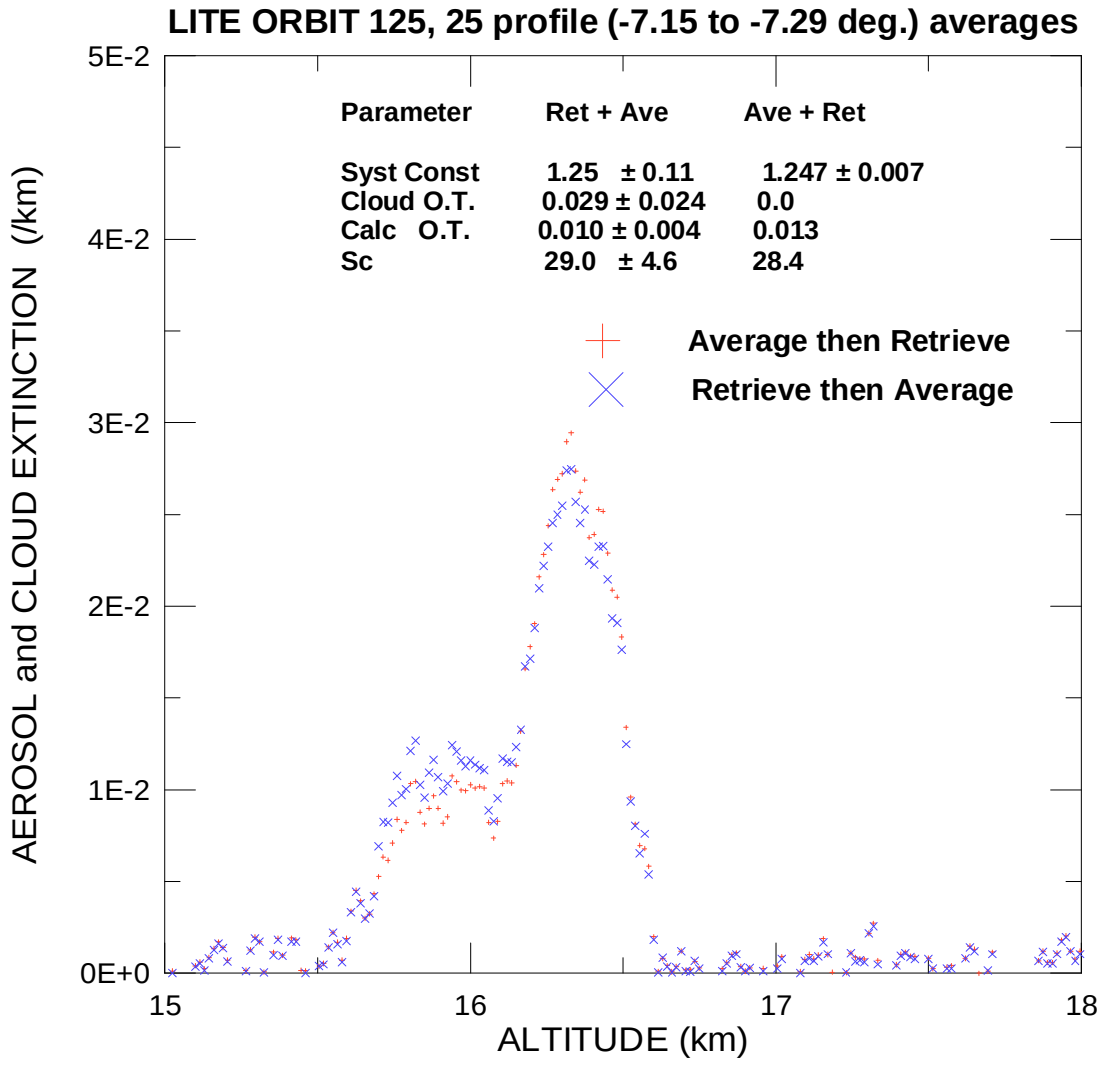

Figure 21. As in Figure 20, but on an expanded scale to show detail of cloud retrieval.

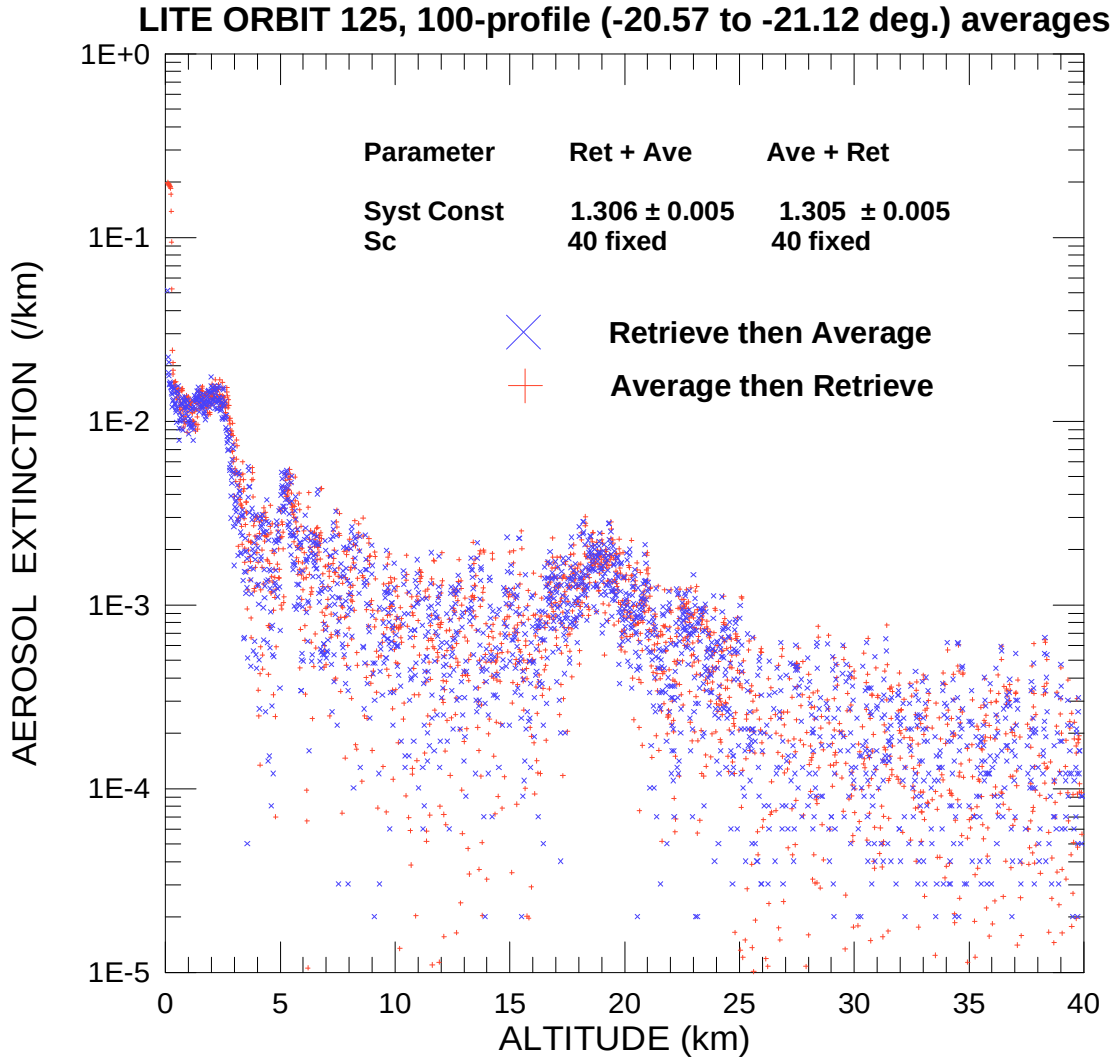

Figure 22. Comparison of "retrieve then average" with "average then retrieve" calculations of the average extinction profile for LITE Orbit 125, over the latitude range –20.572 to –21.115 degrees.

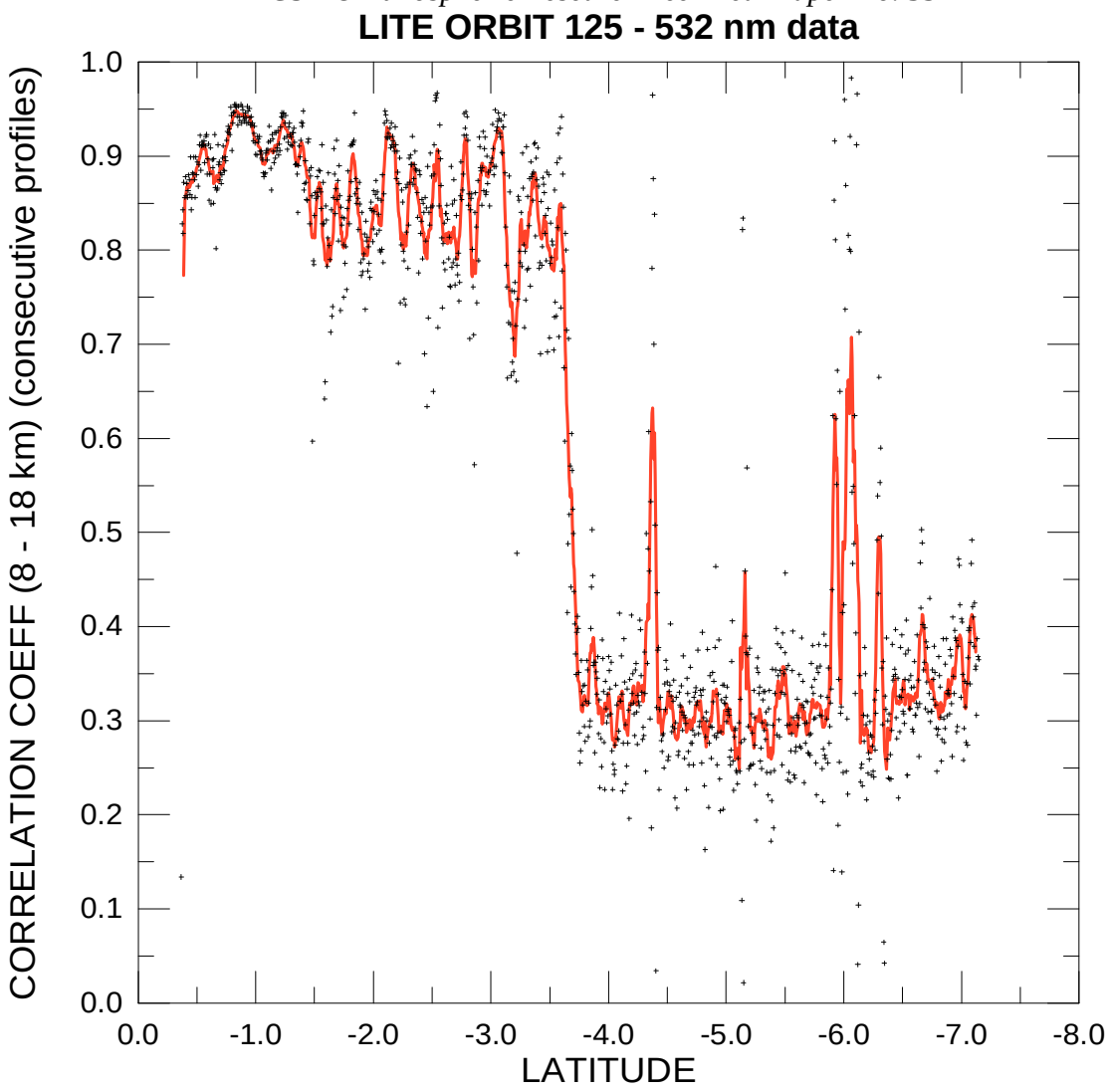

Figure 23. Correlation coefficients calculated over the altitude range 8 to 18 km, for consecutive lidar profiles shown in Figure 6 for LITE Orbit 125. The solid line is a 9-point running mean. The changes in the correlation coefficient can be clearly related to the cloud structure in Figure 6.

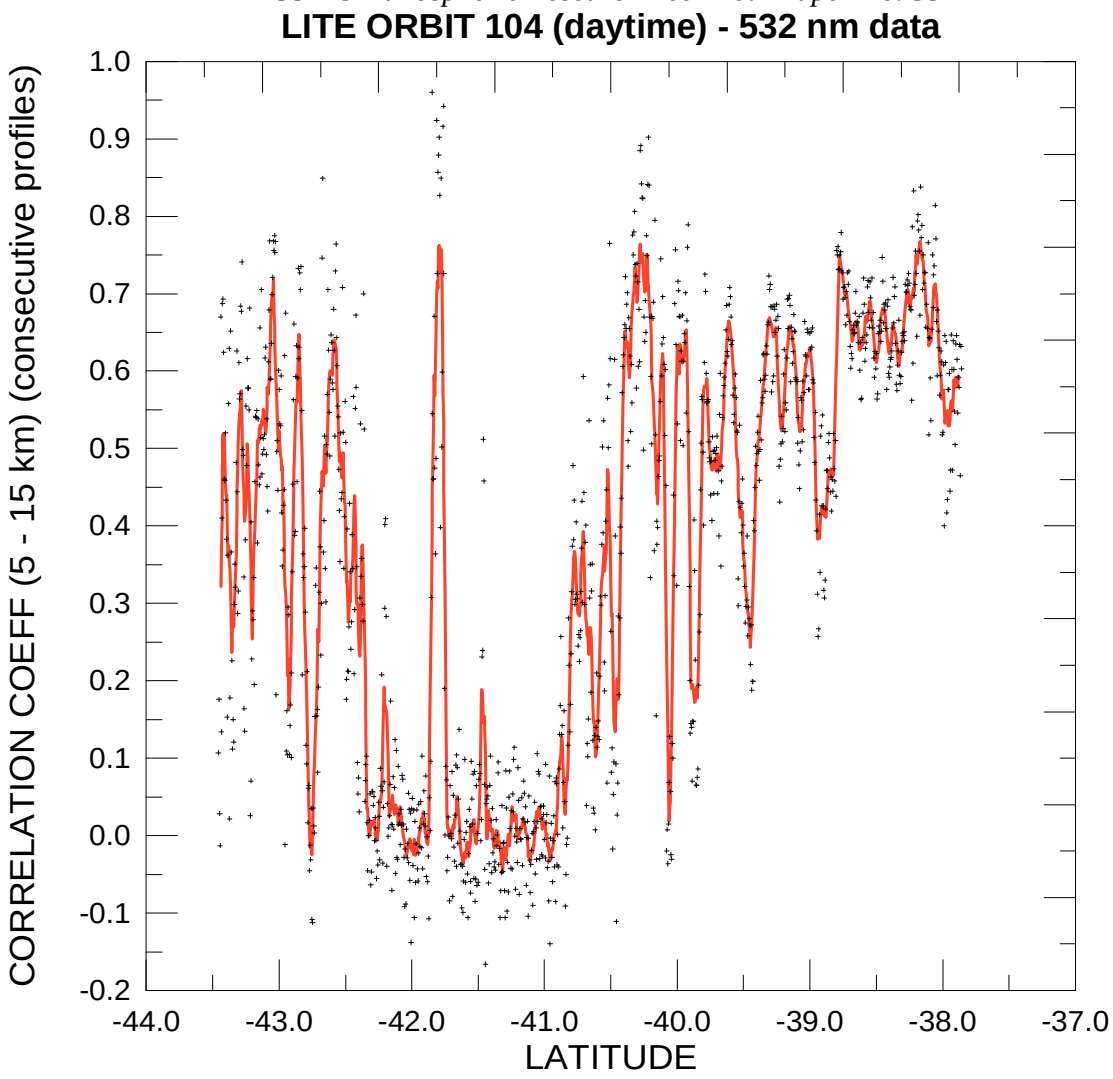

Figure 24. Correlation coefficients calculated over the altitude range 5 to 15 km, for consecutive lidar profiles shown in Figure 12 for LITE Orbit 104. The solid line is a 9-point running mean. The changes in the correlation coefficient can be clearly related to the cloud structure in Figure 12.

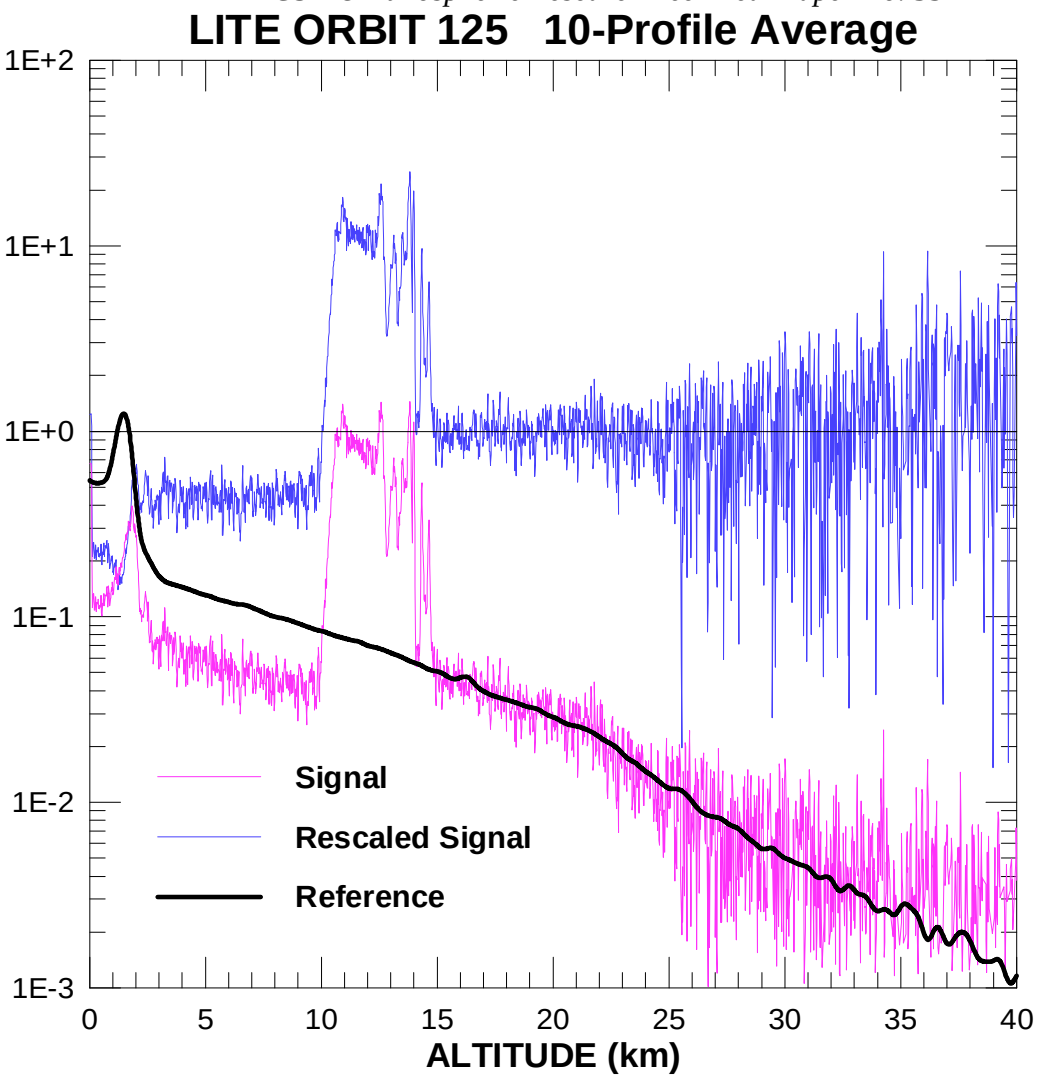

Figure A1-1. The signal profile (magenta) is fitted and rescaled to the reference profile (black) over the altitude range 15 km to 40 km. The ratio of the signal, rescaled to the reference profile, divided by the reference profile is the attenuated scattering ratio (blue).

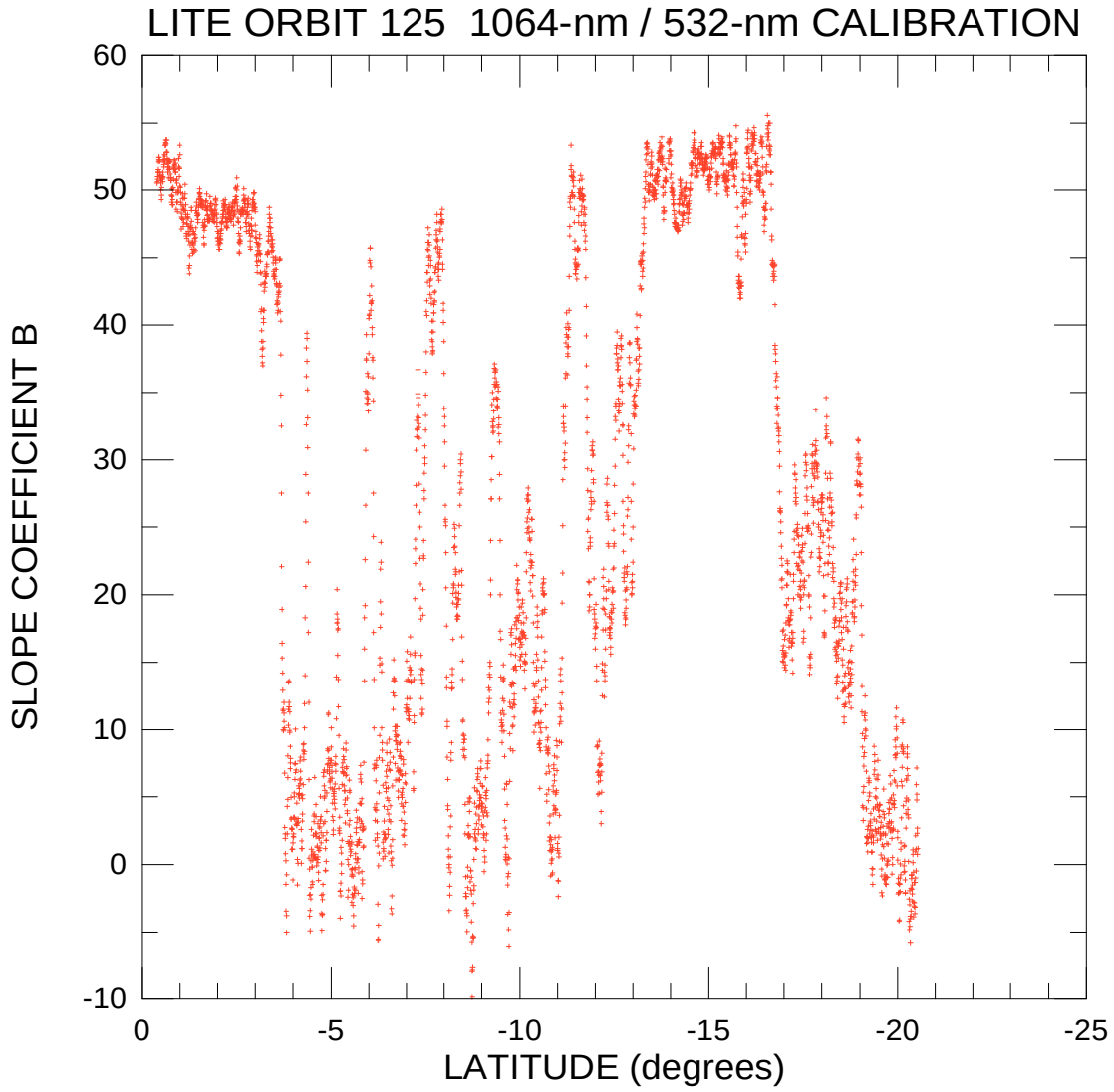

Figure A2-1. The slope coefficient of the linear regression of 1064-nm data points to the corresponding 532-nm points for all data points between 7.5 km and 17.5 km.

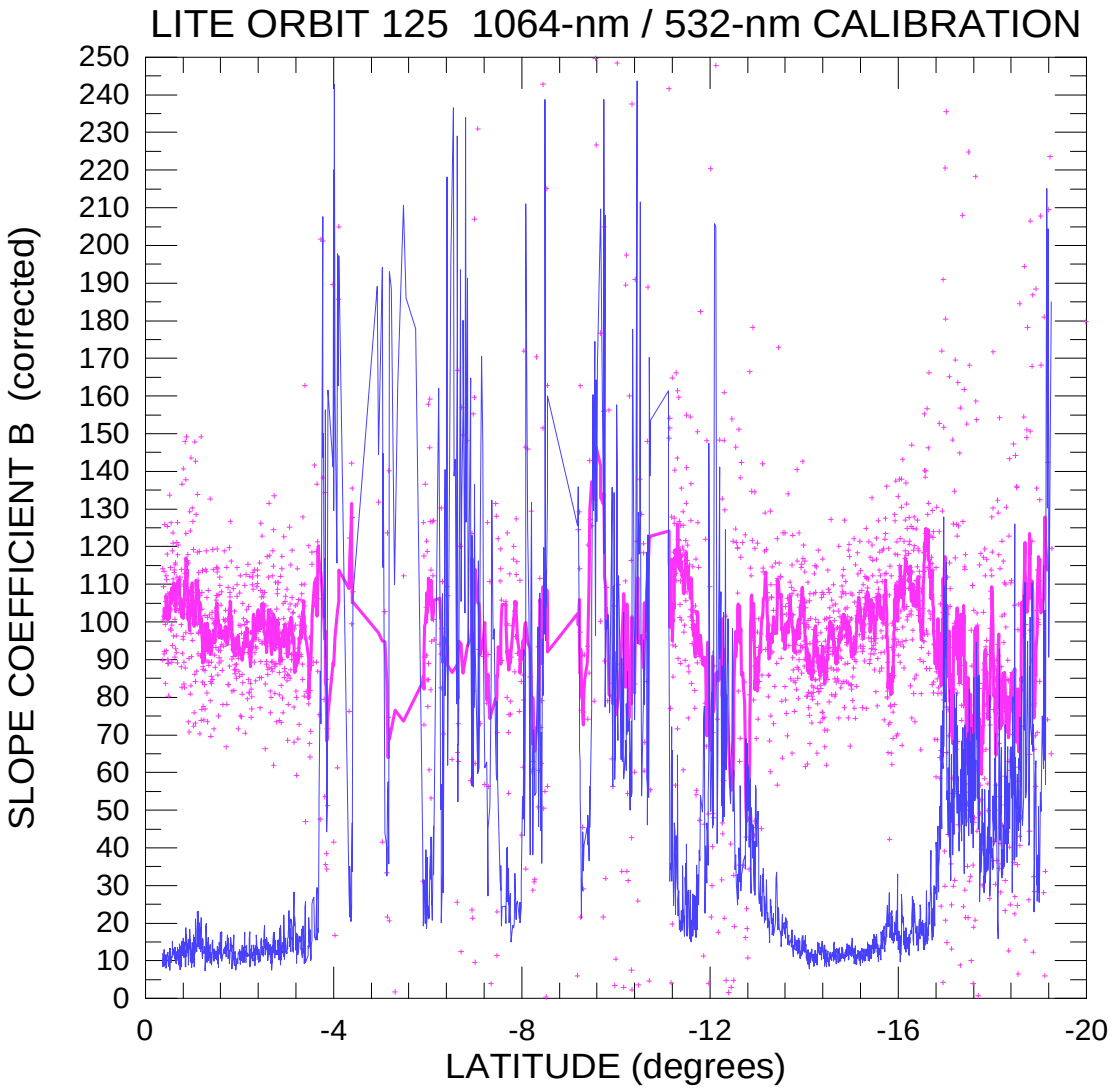

Figure A2-2. The slope coefficient of the linear regression of 1064-nm signals to the corresponding 532-nm signals for data points in cloud regions. The data have been corrected for molecular and ozone attenuation and the 532-nm data have had the aerosol and molecular background level, as attenuated by the cloud, removed before the fit. The magenta (+) points represent the value of B for each individual profile and the heavy magenta line is the running mean over 11 consecutive profiles. The thin blue line is the uncertainty in B.

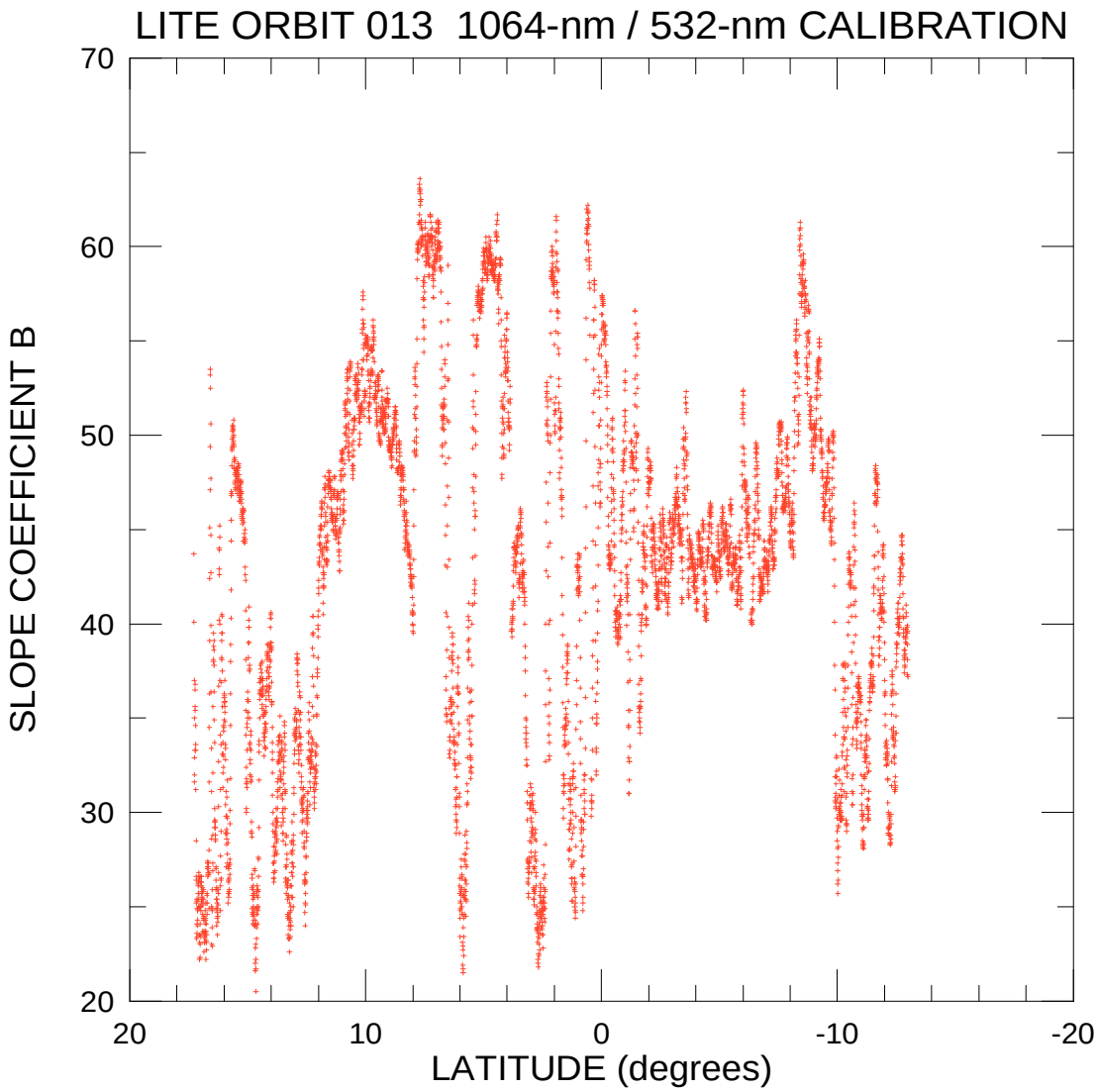

Figure A2-3. The slope coefficient of the linear regression of 1064-nm points to the corresponding 532-nm points for signals between 5.0 km and 17.5 km.

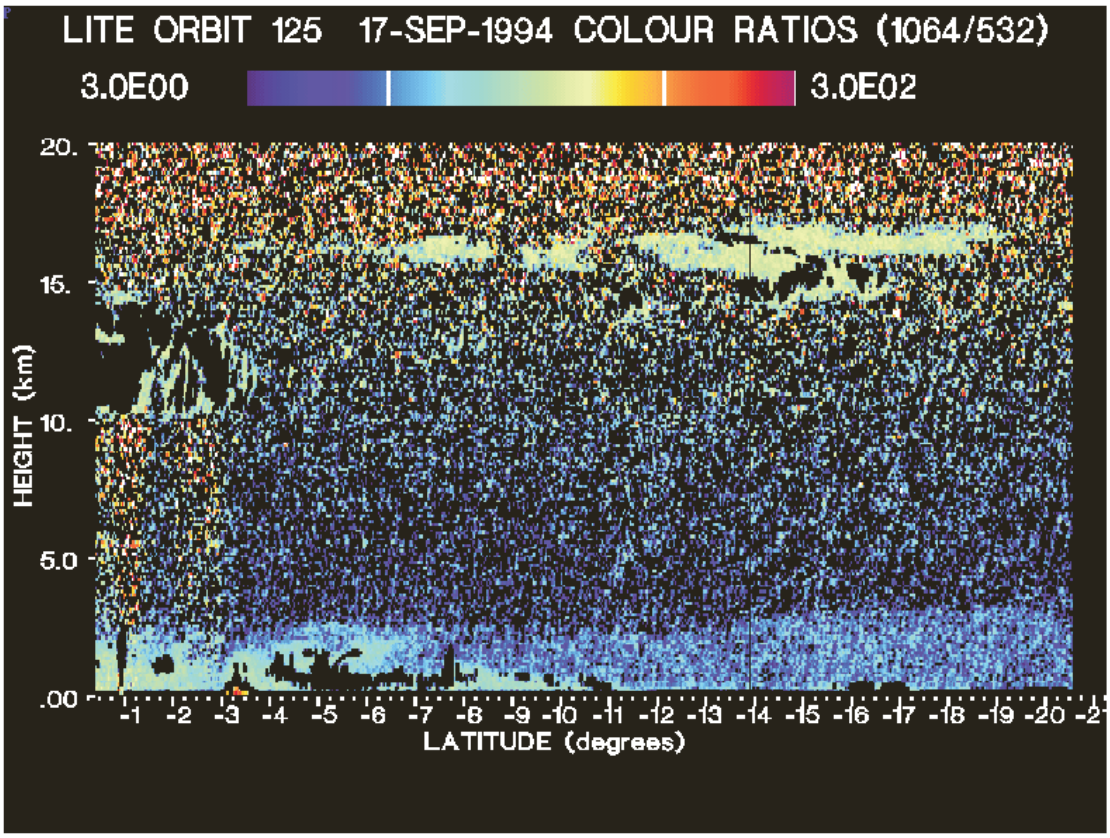

Figure A2-4. Ratios of signals at 1064 nm to those at 532 nm. Signals have been corrected for molecular and ozone attenuation. A 10-profile running mean and a 105-m vertical smoothing have been used. The logarithmic colour scale covers the range 3.0 to 300.

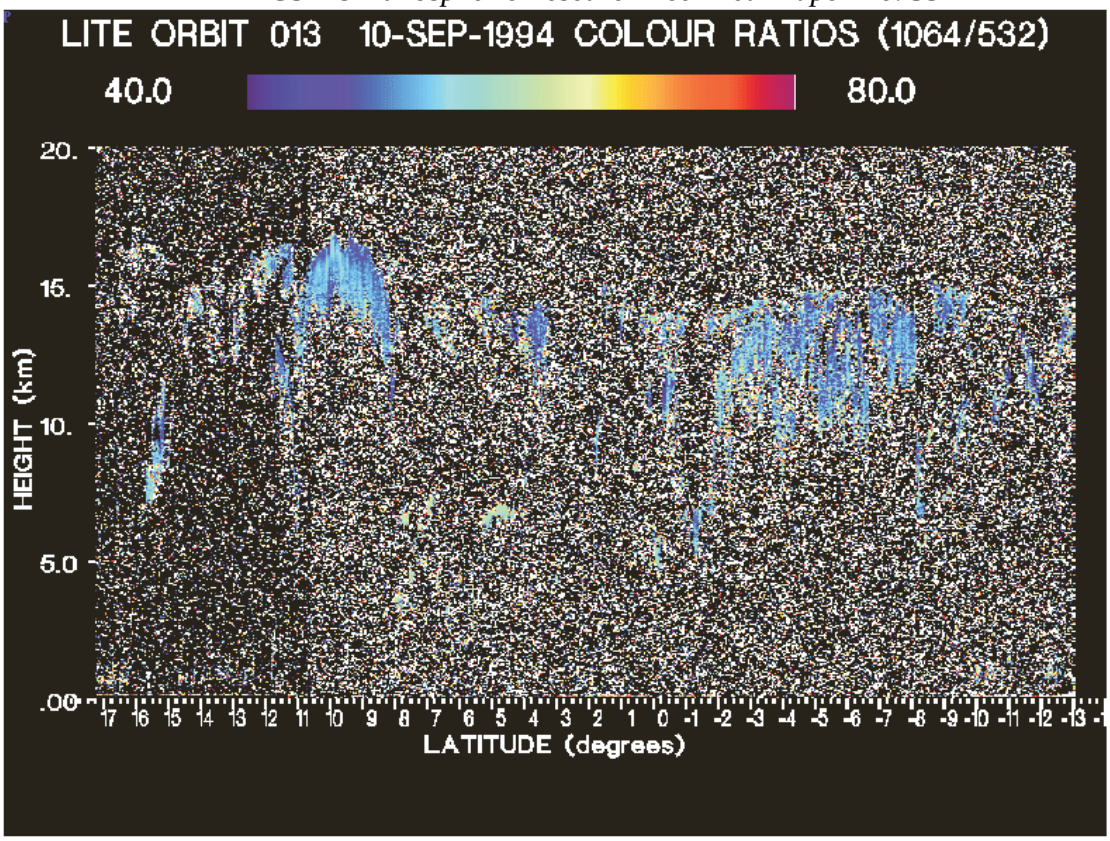

Figure A2-5. Ratios of signals at 1064 nm to those at 532 nm. Signals have been corrected for molecular and ozone attenuation. A 10-profile running mean has been used to smooth the data. The colour scale is linear.

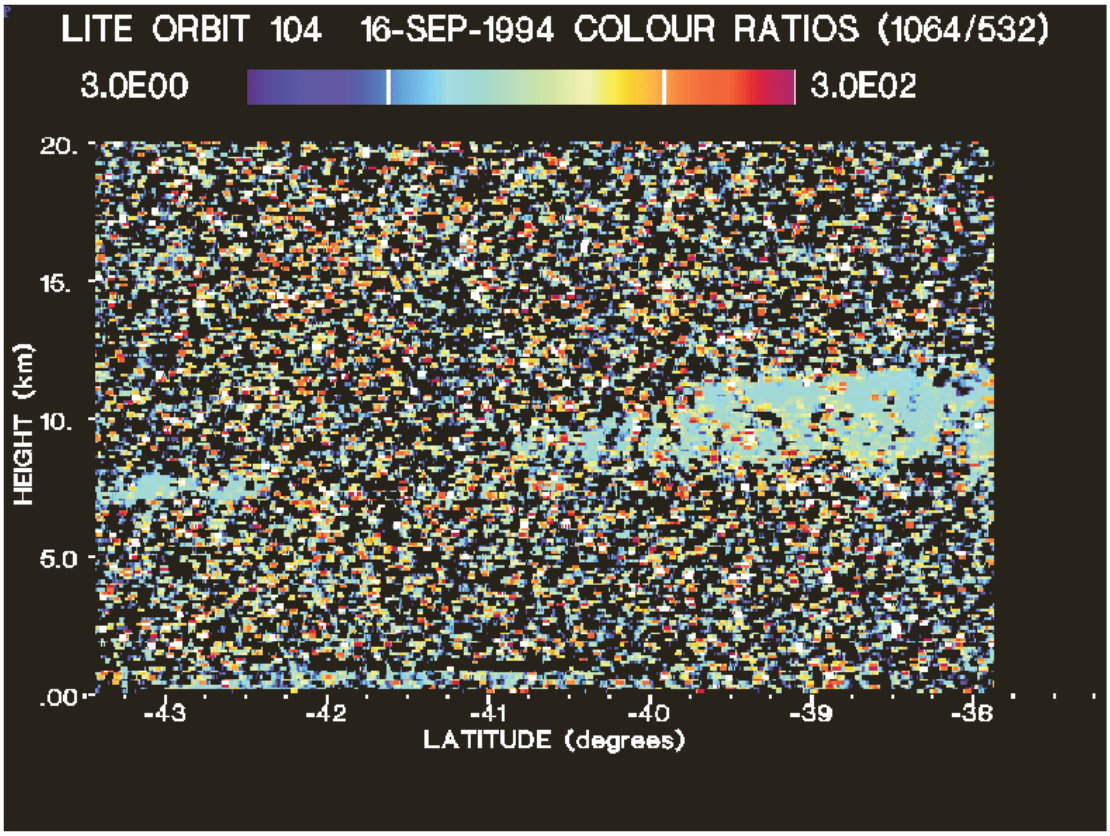

Figure A2-6. Ratios of signals at 1064 nm to those at 532 nm. Signals have been corrected for molecular and ozone attenuation. A 10-profile running mean and a 105-m vertical smoothing have been used. The logarithmic colour scale covers the range 3.0 to 300.

Name	N ave	N smooth	Rcal1	Rcal2	Rcal	SK	dSK	ZB	Zbe	ZT	Zte	Sc	Sce	dSce	τ	ητ e	d ητ	σ	σ e	
FB200011	1	1	665.145	685.02	692.805	5.41E-07	9.70E-08	**10.00**	9.975	**12.00**	12.135	**44.3**	33.0	16.3	**0.5**	0.257	0.197	**0.25**	0.157	
FS200011	1	1	665.145	685.02	692.805	5.41E-07	9.70E-08		9.975		12.135		33.0	16.3		0.257	0.197		0.157	
FS200015	1	5	665.145	685.02	692.565	5.41E-07	9.70E-08		9.975		12.135		33.7	15.5		0.257	0.197		0.157	
FS200201	20	1	665.145	685.02	692.925	5.25E-07	2.33E-08		9.915		12.015		42.1	3.5		0.406	0.063		0.371	
FS202201	20	1	665.145	685.02	692.925	5.25E-07	2.33E-08		10.035		12.015		44.0	3.5		0.434	0.067		0.233	
BS202201	20	1	700.005	704.01	695.025	5.25E-07	2.34E-08		10.035		12.015		42.9	3.2		0.434	0.066		0.233	
LS200201	20	1	665.145	685.02	692.925	5.25E-07	2.34E-08		9.915		12.015		42.4	3.5		0.406	0.063		0.371	
FS204001	400	1	665.145	685.02	692.925	5.09E-07	5.23E-09		9.974		12.015		46.1	0.7		0.503	0.017		0.300	
LS204001	400	1	665.145	685.02	692.925	5.09E-07	5.23E-09		9.975		12.015		46.4	0.7		0.503	0.017		0.299	
FS210011	1	1	665.145	685.02	685.965	5.90E-07	1.02E-07	**10.00**	9.975	**15.00**	18.975	**59.5**	68.0	11.6	**1.5**	2.107	2.053	**0.3**	0.182	
FS210015	1	5	665.145	685.02	689.625	4.34E-07	6.22E-08		9.854		15.075		51.5	7.6		1.762	2.221		0.323	
FS21001a	1	1	665.145	685.02	689.925	5.87E-07	1.02E-07		9.975		15.015		70.5	12.1		2.105	2.053		0.361	
FS21001b	1	1	665.145	685.02	689.925	4.69E-07	1.06E-07		10.155		15.015		67.9		?	67.92		?	2.270	ATTEN
FS210201	20	1	665.145	685.02	689.925	5.15E-07	3.10E-08		10.035		15.015		60.7	3.7		1.472	0.236		0.312	
FS214001	400	1	665.145	685.02	689.925	4.91E-07	6.27E-09		9.974		15.015		59.9	0.8		1.517	0.049		0.302	
FS220011	1	1	665.145	685.02	689.145	5.34E-07	8.92E-08	**14.00**	6.855	**16.00**	15.795	**139.29**	211.1	77.0	**0.3**	0.531	0.499	**0.15**	0.073	
FS220015	1	5	665.145	685.02	688.725	4.84E-07	2.38E-08		14.055		15.975		258.0	21.0		0.592	0.124		0.295	
FS220201	20	1	665.145	685.02	688.965	4.56E-06	3.89E-08		14.170		15.975		152.2	17.6		0.357	0.057		0.147	
BS220201	20	1	700.485	704.91	690.885	4.56E-07	3.90E-08		14.175		15.975		154.6	17.9		0.357	0.057		0.147	
FS224001	400	1	665.145	685.02	688.965	5.21E-07	1.46E-08		14.000		15.980		153.0	5.6		0.339	0.016		0.153	
BS224001	400	1	700.485	704.91	691.065	5.21E-07	1.47E-08		13.995		15.975		153.8	5.7		0.339	0.016		0.153	
FS234001	400	1	665.145	685.02	685.905	4.78E-07	9.57E-09	**14.00**	14.000	**19.00**	19.04	**193.96**	193.2	0.9	**0.75**	0.783	0.017	**0.15**	0.132	
FS270011	1	1	665.145	684.57	691.905	4.44E-07	7.51E-08	**10.00**	10.815	**13.00**	13.035	**50.34**	45.01	?	**4.5**	2.587	?	**1.5**	3.5	ATTEN
FS270201	20	1	665.145	684.57	691.905	4.35E-07	2.46E-08		10.335		13.035		49.403		?	3.21		?	4.02	ATTEN
FS274001	400	1	665.145	684.57	691.905	5.08E-07	6.40E-09		10.035		13.035		53.32	0.68		3.712	1.287		1.514	

NOTES

NOTES

1	Name:	The first letter describes the algorithm used in the retrieval. F means Forward, Fernald, B means Backward Fernald and L means forward Linear Iterative algorithm. The second letter describes the variable derived. B means Backscatter, while S means Sigma (Extinction). The third and fourth letters define the PICASSO-CENA simulation directory. The 5th,6th and 7th characters describe the number of profiles that were avraged The last character describes the number of points smoothing
2	Nave	The number of averaged profiles
3	Nsmooth	The vertical smoothing width. A gaussian weighted smoothing window was used. Nsmooth is twice the standard deviation of the guassian function.
4	Rcal1,2	The calibration was performed by fitting the measured profiles to a modelled molecular backscatter profile over the range Rcal1 to Rcal2. The final point used for calibratio, Rcal, was selected after the cloud boundaries had been established.
5	SK, dSK	This is the System constant and uncertainty, derived from the fitting procedure described in 4.
6	ZB, Zbe	ZB is the simulated cloud base and Zbe is the estimated value produced by the cloud finding algorithm.
7	ZT , Zte	ZT is the simulated cloud top and Zte is the estimated value from the cloud finding algorithm.
8	Sc, Sce	Sc is the simulated value of the Cloud Extinction to Backscatter ratio or lidar ratio. Sce and dSce are the estimated value and associated uncertainty.
9	τ, $\eta\tau$e, d$\eta\tau$	These are, respectively, the simulated optical thickness of the cloud and the estimated value and its uncertainty.
10	σ, σe	These are the simulated average extinction and the retrieved value.
11		All uncertainties are one standard deviation.